

ADA068003

DDC FILE COPY

am
he

① LEVEL III

DDC
RECEIVED
MAY 1 1979
RECEIVED
B

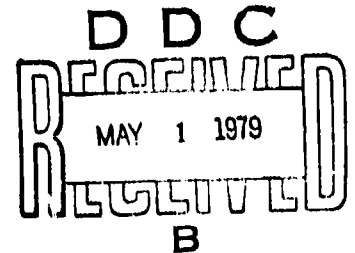
DISTRIBUTION STATEMENT A

Approved for public release;
Distribution Unlimited

University of Oklahoma
School of Aerospace, Mechanical and Nuclear Engineering
Research Report No. OU-AMNE-78-11

LIFTING BODIES DERIVED FROM
SUPERSONIC FLOWS PAST INCLINED
CIRCULAR AND ELLIPTIC CONES

by
Maurice L. Rasmussen



Prepared for
USAF Office of Scientific Research under
GRANT AFOSR 77-3468
OU ORA 158-005
December 1978

DISTRIBUTION STATEMENT A
Approved for public release;
Distribution Unlimited

ADDITIONAL INFORMATION: THIS REPORT IS AVAILABLE FROM THE
ADVISORY BOARD ON AERONAUTICS AND SPACE (AFSC)
ATTENTION: TECHNICAL REPORTS
1215 GREENBELT ROAD
GREENBELT, MARYLAND 20740
DISTRIBUTION STATEMENT A (7b)
AERONAUTICAL INFORMATION OFFICER

ABSTRACT

Lifting-body configurations are constructed from stream surfaces generated by means of supersonic flows past inclined circular and elliptic cones. By such means waverider shapes are devised with curved surfaces and known pressure fields and shock-layer structures. The conical flow fields stem from perturbations of the basic axisymmetric cone flow arising from small angle of attack and small cross-section eccentricity. The approximate results are analytic and in the form of hypersonic small disturbance theory. Various possibilities for waverider shapes are discussed. Design formulas are presented that determine how the Mach number, angle of attack, cross-section eccentricity, and characteristic cone angle affect the waverider shape, pressure distribution, and shock-layer structure.

APPROVED	
DATE	
BY	
DISPATCHED	
BY	
DATE	
A	

ACKNOWLEDGEMENTS

This investigation was sponsored by the United States Air Force, under Grant No. 77-3468. Thanks go to Dr. Donald Daniel, the project monitor, for his interest and encouragement. Many enlightening discussions with Professor Martin Jischke are also gratefully acknowledged.

TABLE OF CONTENTS

	<u>Page</u>
ACKNOWLEDGEMENTS	iii
LIST OF ILLUSTRATIONS	vi
LIST OF SYMBOLS	viii
1. INTRODUCTION	1
2. FUNDAMENTAL WEDGE-DERIVED WAVERIDER	4
3. GENERAL CONSIDERATIONS FOR CONICAL FLOWS	8
3.1 Coordinates and Geometry	8
3.2 Shock-Layer Structure	9
3.3 Conical Stream Surfaces	10
4. WAVERIDERS DERIVED FROM INCLINED CIRCULAR CONES	18
4.1 Stream Surfaces	18
4.2 Approximate Integration	18
4.3 Lip Angle	20
4.4 Spacing of the Stream Surfaces	21
4.5 Waveriders with a Freestream Upper Surface	22
4.6 Waveriders with a Complementary Wedge Surface	25
5. WAVERIDERS DERIVED FROM ELLIPTIC CONES	42
5.1 Stream Surfaces	42
5.2 Approximate Integration	43
5.3 Lip Angle	44
5.4 Waveriders with a Freestream Upper Surface	44
6. WAVERIDERS DERIVED FROM INCLINED ELLIPTIC CONES	50
6.1 Stream Surfaces	50
6.2 Maximum-Entropy Surface	52
6.3 Lip Angle	53
6.4 Waveriders with Freestream Upper Surfaces	54
6.5 Further Remarks	55
7. SOME CONSIDERATIONS REGARDING CONTROL SURFACES	59
7.1 Control Flaps	59
7.2 Vertical-Fin Control Surfaces	59
7.3 Vertical Fin for the Elliptic-Cone Waverider	61
7.4 Vertical Fin for Inclined-Cone Waveriders	62
8. CONCLUDING REMARKS	66

	<u>Page</u>
REFERENCES	68
APPENDIX A: FORMULAS FOR THE BASIC AXISYMMETRIC CONE FLOW	70
APPENDIX B: FORMULAS FOR INCLINED ELLIPTIC CONE FLOW PERTURBATIONS	72

LIST OF ILLUSTRATIONS

	<u>Page</u>
Figure 2.1 a) Wedge-Shock Configuration b) Wedge-Derived Waverider	7
Figure 3.1 Cone Coordinates and Geometry	12
Figure 3.2 Shock Eccentricity Factors, $\gamma = 1.4$	13
Figure 3.3 Inclined-Cone Velocity Perturbations a) radial b) polar c) azimuthal	14
Figure 3.4 Elliptic-Cone Velocity Perturbations a) radial b) polar c) azimuthal	15
Figure 3.5 Azimuthal Velocity at the Body Surface	16
Figure 3.6 Surface Pressure Perturbations	17
Figure 4.1 Circular-Cone Stream-Surface Function	28
Figure 4.2 Circular-Cone Lip Angle	29
Figure 4.3 Stream Surfaces For Inclined Cone	30
Figure 4.4 Circular-Cone Waverider With Freestream Upper Surface: Positive Dihedral	31
Figure 4.5 Circular-Cone Waverider With Freestream Upper Surface: Zero Dihedral	32
Figure 4.6 Circular-Cone Waverider With Freestream Upper Surface: Negative Dihedral	33
Figure 4.7 Circular-Cone Waverider With Wedge-Shock Upper Surface	34
Figure 4.8 α/δ Versus K_δ For Various Dihedral Angles	35
Figure 4.9a Wedge Shock-Circular Cone Waveriders, $\alpha/\delta = 0.1$	36
Figure 4.9b Wedge Shock-Circular Cone Waveriders, $\alpha/\delta = 0.2$	37
Figure 4.9c Wedge Shock-Circular Cone Waveriders, $\alpha/\delta = 0.3$	38

	<u>Page</u>
Figure 4.9d Wedge Shock-Circular Cone Waveriders, $\alpha/\delta = 0.4$	39
Figure 4.9e Wedge/Shock-Circular Cone Waveriders, $\alpha/\delta = 0.5$	40
Figure 4.9f Wedge Shock-Circular Cone Waveriders, $\alpha/\delta = 0.6$	41
Figure 5.1 Stream Surfaces for Elliptic Cone	46
Figure 5.2 Elliptic-Cone Stream-Surface Function	47
Figure 5.3 Elliptic-Cone Lip Angle	48
Figure 5.4 Elliptic Cone Waveriders With Freestream Upper Surfaces	49
Figure 6.1 Stream Surfaces for Inclined Elliptic Cone	56
Figure 6.2 Azimuthal Velocity Ratios at Shock and Body	57
Figure 6.3 Inclined Elliptic-Cone Waverider With Freestream Upper Surface: Positive Dihedral	58
Figure 7.1 Geometry for the Vertical Fin	63
Figure 7.2 Elliptic-Cone Waverider with Fin Starting at Vertex	64
Figure 7.3 Elliptic-Cone Waverider with Fin Starting at Half Length	65

LIST OF SYMBOLS

a	tangent of semivertex angle of semiminor axis
b	tangent of semivertex angle of semimajor axis
C_{p_0}	pressure coefficient for basic circular cone
\tilde{C}_{p_1}	perturbation pressure coefficient for angle of attack
C_{p_1}	perturbation pressure coefficient for cross-section eccentricity
e	eccentricity factor for elliptic cone
\tilde{g}	angle-of-attack shock eccentricity factor
g	elliptic-cone shock eccentricity factor
K_δ	hypersonic similarity parameter, $M_\infty \delta$
M_∞	freestream Mach number
\hat{n}	unit normal vector
r, θ, ϕ	spherical curvilinear coordinates
s	entropy
u_0, v_0	radial and polar velocity components associated with basic circular cone
$\tilde{u}_1, \tilde{v}_1, \tilde{w}_1$	spherical velocity-component perturbations associated with angle of attack
u_1, v_1, w_1	spherical velocity-component perturbations associated with elliptic cone
α	angle of attack
β	unperturbed shock angle
γ	ratio of specific heats
δ	semivertex angle of basic circular cone
ϵ	perturbation parameter for cross-section eccentricity
ξ_0	density ratio across basic shock
ρ	density
σ	β/δ

LIFTING BODIES DERIVED FROM
SUPERSONIC FLOWS PAST INCLINED CIRCULAR
AND ELLIPTIC CONES

1. Introduction

The design of an aircraft for high supersonic flight that achieves desirable aerodynamic behavior and still accommodates such demands as propulsion, structures, materials, and operations is a very challenging task. A discussion of the requirements of hypersonic aircraft is given by Küchemann [1] and by Küchemann and Weber [2]. When the Mach numbers are sufficiently high that the flow disturbances are intrinsically nonlinear, a treatment of the problem by means of linearized theory is not appropriate. A generalized study of the problem by means of numerical solutions of the nonlinear governing equations of fluid mechanics is very formidable indeed. For this reason the few known exact solutions for flows past elementary geometries are extremely important. These basic exact solutions provide insight and a knowledge of fundamental physical features associated with high-speed flow. In addition, they can also be used as building blocks for flows past more complex geometries.

A basic scheme for deriving exact solutions for three-dimensional lifting bodies by means of simple two-dimensional wedge flows was set forth by Nonweiler [3]. These results were elaborated upon by Venn and Flower [4], Nardo [5], and others. The simplest configurations thus derived are called caret wings, or caret waveriders, because of their caret shape. Because these aerodynamic shapes are derived from basic two-dimensional flows, they generally involve flat surfaces and concomitant sharp corners where these surfaces intersect. These sharp corners may be undesirable when factors such as viscous and heating effects are taken into account.

Corresponding to the flat surfaces generated by the basic wedge-shock flow, curved surfaces can be generated by utilization of the stream surfaces associated with the axisymmetric supersonic flow past a circular cone. Such surfaces were devised by Jones [6] and Woods [7]. These constructions generate curved surfaces and curved shocks that are attached to sharp leading edges. The flows for both the cone-generated surfaces and the wedge-generated surfaces can be classified as conical flows.

Besides the axisymmetrical conical flows, there are also conical flows associated with inclined circular cones and with non-circular cones. These flows generate stream surfaces that could be attractive for constructions of lifting bodies with curved surfaces. The analytical description of these flows, as contrasted with a numerical description, generally involves a perturbation analysis of the basic axisymmetric circular-cone flow. A straight-forward perturbation analysis is not uniformly valid in all the variables, but fails in a vortical layer adjacent to the body surface. The pressure and azimuthal velocity, however, are uniformly valid across the vortical layer [8,9,10]. This is very important because the azimuthal perturbation velocity is pertinent in determining the flow stream surfaces and the pressure is important in determining the relevant forces on the surfaces. Thus the first-order straight-forward perturbation expansion, while being suspect at first glance, is thus pertinent in determining the stream surfaces and related forces on waverider configurations generated by the perturbation results. The object of this investigation is to generate various waverider configurations by means of angle-of-attack and cross-section eccentricity perturbations of the basic axisymmetric cone flow.

The present study rests heavily on the fact that approximate analytical expressions are available for the perturbed flows past circular [11,12] and

elliptic [13,14] cones at small angle of attack. These results allow for an analytical, as opposed to a numerical, investigation to be performed that leads to results that are simple and easily understood. The effects of free-stream Mach number, pertinent cone angle, angle of attack, cross-section eccentricity, and ratio of specific heats on the shock shape, shock-layer structure, stream-surface shape, and surface conditions can be readily established. Although the results are approximate, they are accurate enough for the parametric and design considerations that are of primary concern here. When the trends and concepts have become clear, more precise and elaborate schemes of analysis can be undertaken for numerical accuracy.

Our main concern in this paper is the generation of stream surfaces that can be used as solid surfaces in lifting-body waverider configurations. We shall outline how the pressure distributions can be obtained, but we shall not obtain actual lift, drag, or moment results here. Such results, and other results of interest such as reported by Squire [15], will be the subject of further research.

2. Fundamental Wedge-Derived Waverider

The fundamental wedge-derived waverider, sometimes called the caret waverider, is derived from the basic exact flow field produced by supersonic flow through a plane oblique shock wave, as shown in Fig. 2.1a. The flow is deflected by the angle Δ when passing through the shock. The plane shock wave is inclined at an angle β with the freestream flow. Let the line formed by the common intersection of the planes parallel and perpendicular to the freestream flow with the plane of the shock denote the leading edge of a solid wedge. The upper surface of the wedge is parallel to the freestream flow and the lower surface of the wedge, inclined downward at an angle Δ with the upper surface, is the stream surface of the flow that has passed through the shock at the common-line intersection denoting the leading edge of the wedge. The flow field between the lower surface of the wedge and the shock wave is parallel and uniform and has properties obtainable from the oblique-shock relations.

The oblique-shock relations are well known and can be expressed in analytical form exactly for a thermally and calorically perfect gas. Owing to the intrinsic interaction of the variables, however, the shock angle, β , cannot be obtained explicitly as a function of the deflection angle, Δ . It is thus useful to utilize the approximate results of hypersonic small disturbance theory, valid for large freestream Mach numbers, M_∞ , and small deflection and shock angles. This shock-angle relation originally obtained by Linnell [16] is

$$\frac{\sin \beta}{\sin \Delta} = \frac{\gamma+1}{4} + \sqrt{\left(\frac{\gamma+1}{4}\right)^2 + \frac{1}{(M_\infty \sin \Delta)^2}} \quad (2.1)$$

The corresponding relation for the pressure coefficient is

$$C_p \equiv \frac{p - p_\infty}{\frac{1}{2} \rho_\infty V_\infty^2} \quad ,$$

$$\frac{C_p}{(\sin \Delta)^2} = \frac{\gamma+1}{2} + \sqrt{\left(\frac{\gamma+1}{2}\right)^2 + \frac{4}{(M_\infty \sin \Delta)^2}} \quad . \quad (2.2)$$

In inviscid steady flow, any stream surface can be utilized as a solid surface since no flow crosses a stream surface. We now wish to visualize further stream surfaces in Fig. 2.1a and utilize them as solid surfaces in a new configuration. Mark out the axis AB aligned with the freestream flow and lying in the top surface of the wedge. The normal projection of the axis AB onto the lower surface of the wedge is denoted by AC. Any plane passing through the axis AB is aligned with the freestream flow, and any plane passing through the axis AC is aligned with the shock deflected flow. Now select the points D and E on the shock surface, positioned symmetrically (but not necessarily) on either side of the axes AB and AC. The two plane surfaces passing through the pair of three points ACD and ACE are stream surfaces in the shock deflected flow. The two plane surfaces passing through the pairs of three points ABD and ABE are stream surfaces in the freestream flow. If we choose these four new stream surfaces as the relevant solid surfaces of an aerodynamic body, then the new configuration appears as shown in Fig. 2.1b. This aerodynamic configuration is called a caret waverider since it appears to ride on the plane shock wave attached to its under surface. The upper surface is parallel to the free stream and hence at freestream conditions. The under surface of the caret shape is at a uniform pressure given by formula (2.2), and the shock stand-off angle is given by formula (2.1). For a given caret waverider configuration, the shock wave will be

attached as shown in Fig. 2.1b only for the particular Mach number determined from Eq. (2.1) with β and Δ given. The caret waverider is a lifting aerodynamic shape since the pressure is higher on the under surface.

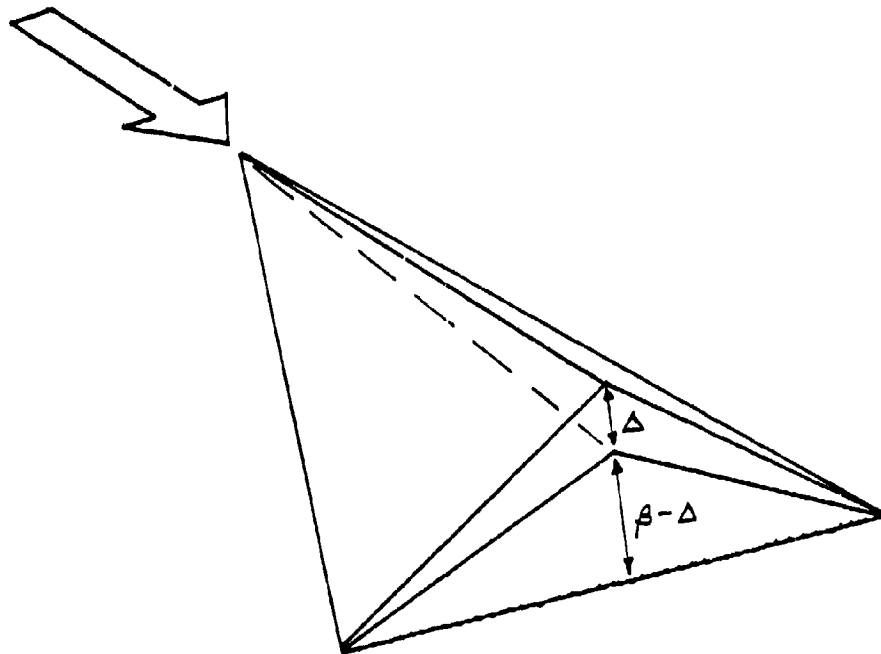
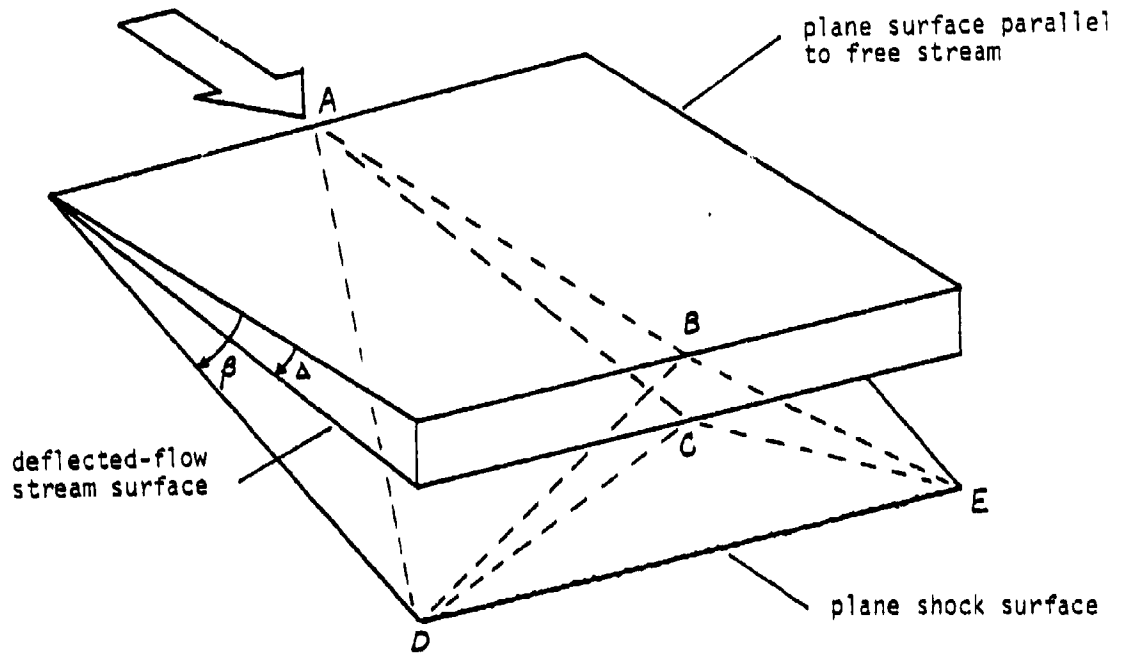


Figure 2.1 a) Wedge-Shock Configuration
b) Wedge-Derived Waverider

3. General Considerations for Conical Flows

3.1 Coordinates and Geometry

We wish to determine the stream surfaces of conical flows past slender elliptic cones at small angles of attack [13,14]. We use spherical coordinates in a body-fixed system shown in Fig. 3.1. Let $a \equiv \tan \theta_a$ and $b \equiv \tan \theta_b$ be the semivertex angles of the semiminor and semimajor axes of the elliptic cone. Then the elliptic cone is described by

$$\tan \theta_c = \frac{\tan \theta_m}{\sqrt{1+e} \cos 2\phi} \quad , \quad (3.1)$$

where

$$\begin{aligned} \tan \theta_m &= \frac{\sqrt{2} ab}{\sqrt{a^2 + b^2}} = b \sqrt{1-e} = a \sqrt{1+e} \quad , \\ &= \sqrt{ab} (1-e^2)^{1/4} \quad , \end{aligned} \quad (3.2a)$$

$$e \equiv \frac{b^2 - a^2}{b^2 + a^2} \quad . \quad (3.2b)$$

The parameter e is a measure of the eccentricity of the elliptic cone. For small eccentricities we can expand Eq. (3.1) in a Fourier series, the first two terms of which are

$$\theta_c = \delta - \epsilon \cos 2\phi + O(\epsilon^2) \quad , \quad (3.3)$$

where

$$\delta \equiv \theta_m + \frac{e^2}{32} [3 - 2 \sin^2 \theta_m] \sin 2\theta_m + O(e^4) \quad , \quad (3.4a)$$

$$\epsilon \equiv \frac{e}{4} [1 + \frac{e^2}{32} (15 - 20 \sin^2 \theta_m + 8 \sin^4 \theta_m) + O(e^4)] \sin 2\theta_m \quad . \quad (3.4b)$$

The parameter ϵ is a new measure of the eccentricity and is the appropriate small parameter in a perturbation procedure. The parameter δ specifies the semivertex angle of the basic circular cone about which the perturbation expansion is performed.

The conical shock wave attached to the elliptic cone has the form [13,14], for small α and ϵ ,

$$\theta_s = \beta + \alpha \tilde{g} \cos \phi - \epsilon g \cos 2\phi \quad , \quad (3.4)$$

where

$$\beta/\delta = \left[\frac{\gamma+1}{2} + \frac{1}{K_\delta^2} \right]^{1/2} \quad , \quad (3.5)$$

and $K_\delta \equiv M_\infty \delta$ is the hypersonic similarity parameter. The parameters \tilde{g} and g are the shock eccentricity factors associated with angle of attack and elliptic cone eccentricity. They are functions of K_δ and are shown in Fig. 3.2.

3.2 The Shock-Layer Structure

Let u , v , and w denote the r , θ , and ϕ spherical components of velocity, and let p denote the pressure. Outside the surface vortical layer and the viscous boundary layer, the variables have the following expansions for small α and ϵ :

$$\begin{aligned} u(\theta, \phi) &= u_0(\theta) + \alpha \tilde{u}_1(\theta) \cos \phi + \epsilon u_1(\theta) \cos 2\phi \\ v(\theta, \phi) &= v_0(\theta) + \alpha \tilde{v}_1(\theta) \cos \phi + \epsilon v_1(\theta) \cos 2\phi \\ w(\theta, \phi) &= \alpha \tilde{w}_1(\theta) \sin \phi + \epsilon w_1(\theta) \sin 2\phi \\ p(\theta, \phi) &= p_0(\theta) + \alpha \tilde{p}_1(\theta) \cos \phi + \epsilon p_1(\theta) \cos 2\phi \end{aligned} \quad (3.6)$$

The lowest-order terms in the expansions, with the subscript zero, pertain to the basic-cone solution. The first-order terms with the tilde notation pertain to the angle-of-attack perturbation, and the first-order terms without

the tilde notation pertain to the elliptic-cone eccentricity perturbation. The pressure and the azimuthal velocity components, $\tilde{w}_1(\theta)$ and $w_1(\theta)$, are uniformly valid across the vortical layer.

As calculated by Doty and Rasmussen [12], the angle-of-attack velocity perturbations $\tilde{u}_1/(V_\infty \delta)$, \tilde{v}_1/V_∞ , and \tilde{w}_1/V_∞ are functions of θ and K_δ within the fabrication of hypersonic small-disturbance theory. Correct to the first order expansion of interest, the shock-layer structure can be normalized by the variable

$$\tilde{\theta} \equiv \frac{\theta - \delta}{\beta - \delta} \quad (3.7)$$

At the cone surface, $\tilde{\theta} = 0$, and at the shock, $\tilde{\theta} = 1$. The angle-of-attack velocity components are shown in Figs. 3.3a, b, c as a function of $\tilde{\theta}$ and various values of K_δ . The corresponding elliptic eccentricity velocity components [13,14] are shown in Figs. 3.4a, b, c. The body-surface values of the azimuthal velocity components, $\tilde{w}_1(\theta_c)$ and $w_1(\theta_c)$, are shown in Fig. 3.5 as a function of K_δ . The body surface perturbation pressure coefficients, \tilde{C}_{p1} and C_{p1} , are shown in Fig. 3.6 as a function of K_δ .

3.3 Conical Stream Surfaces

The vector equation for a streamline, $\vec{V} \times d\vec{s} = 0$, can be written in spherical coordinates as

$$\frac{dr}{u(\theta, \phi)} = \frac{r d\theta}{v(\theta, \phi)} = \frac{r \sin \theta d\phi}{w(\theta, \phi)} \quad (3.8)$$

The conical stream surfaces are determined by the last two terms of Eq. (3.8).

For small angles and to lowest order we have

$$\frac{d\theta}{\theta v_\theta(\theta)} = \frac{d\phi}{\alpha \tilde{w}_1(\theta) \sin \phi + \epsilon w_1(\theta) \sin 2\phi} \quad (3.9)$$

To lowest order, only the zeroth-order polar velocity, $v_0(\theta)$, for the basic cone and the uniformly valid azimuthal perturbation velocities, $\bar{w}_1(\theta)$ and $w_1(\theta)$, enter the analysis. Even though these velocity functions are known, it does not appear possible to obtain an integral of Eq. (3.9) analytically. In the cases when α or ϵ vanish separately, the variables in Eq. (3.9) can be separated, and integration can then be obtained at least by quadratures.

The polar velocity, $v_0(\theta)$, can be approximated accurately for small angles by [11,12,13,14,17]

$$v_0(\theta) = -V_\infty \left(1 - \frac{\delta^2}{\theta^2}\right) \quad (3.10)$$

Other formulas for the basic-cone flow and the perturbed flow are summarized in the Appendix.

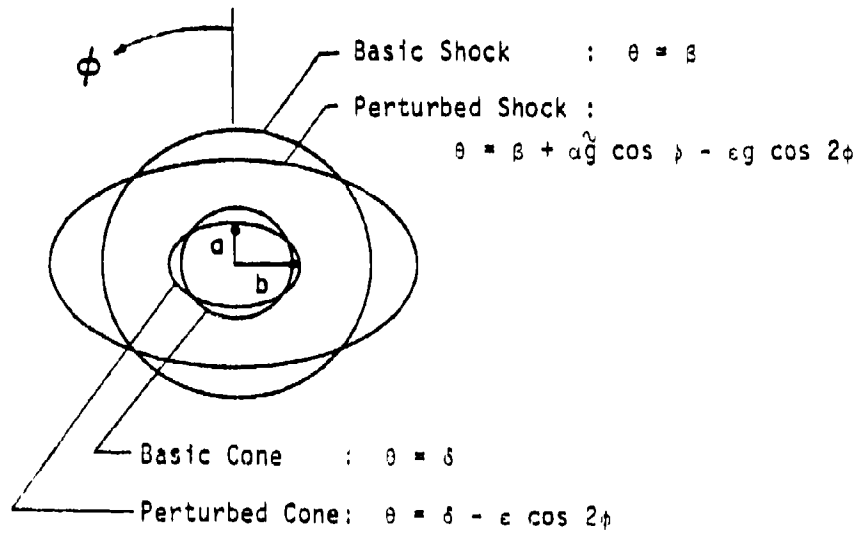
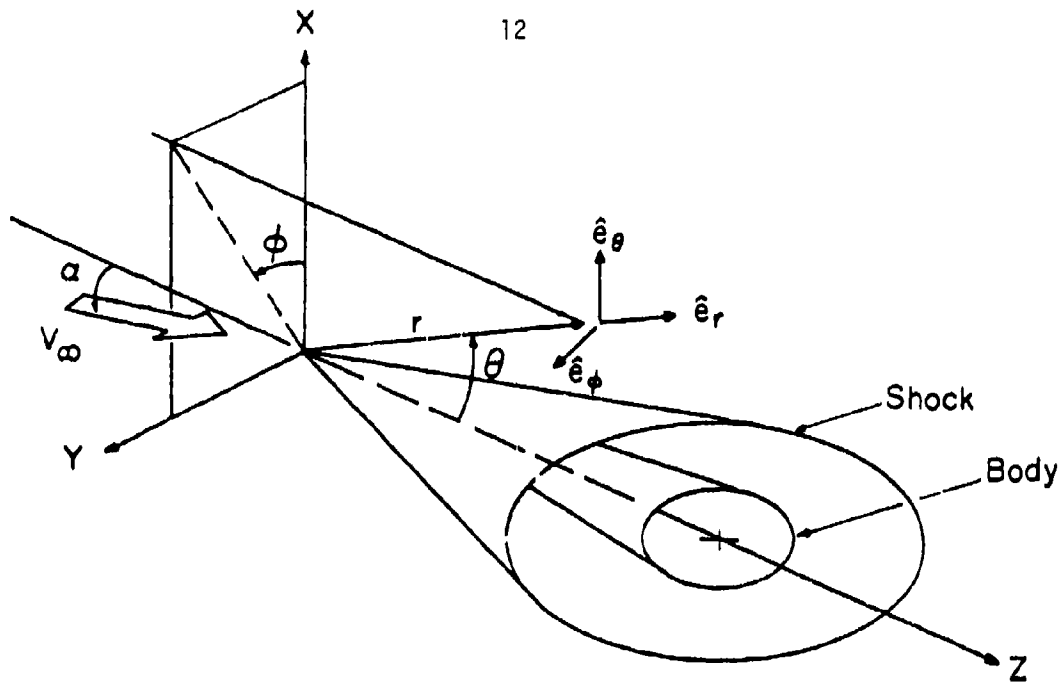


Figure 3.1 Cone Coordinates and Geometry

$$\theta_s = \beta + \alpha \tilde{g} \cos \phi - \epsilon g \cos 2\phi$$

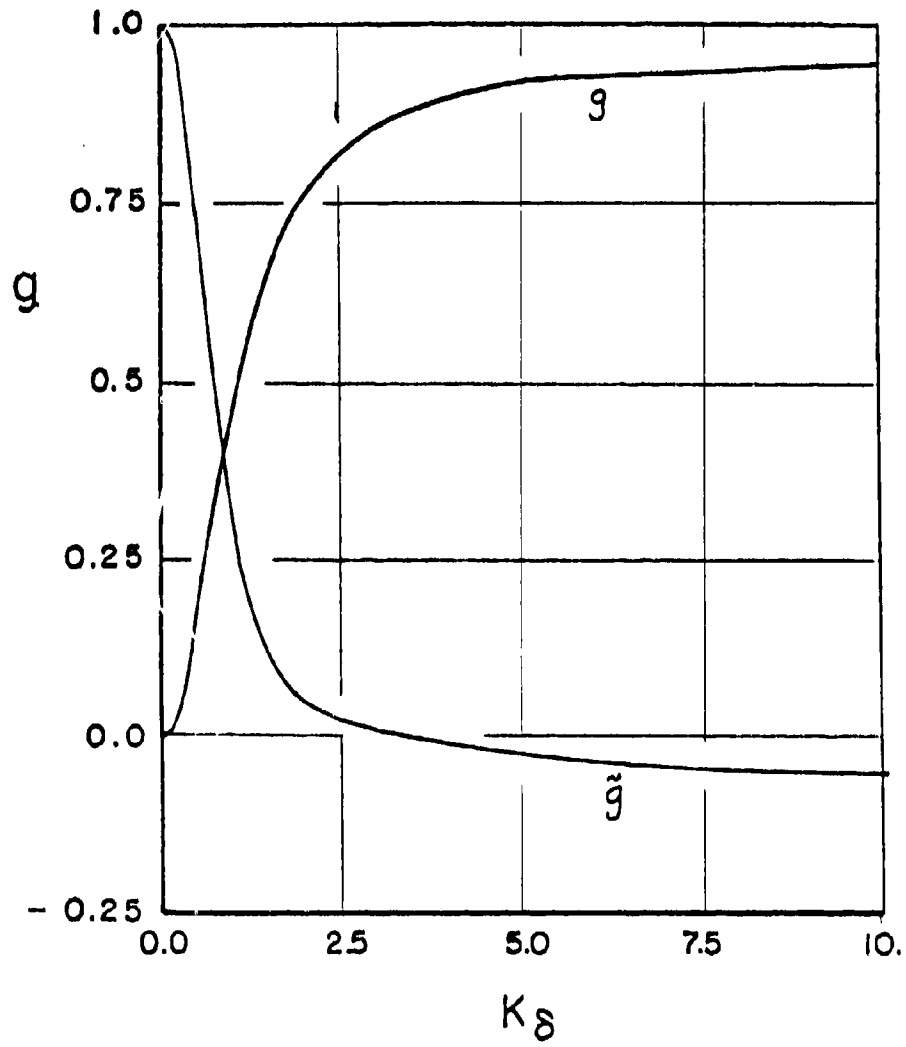


Figure 3.2 Shock Eccentricity Factors, $\gamma = 1.4$

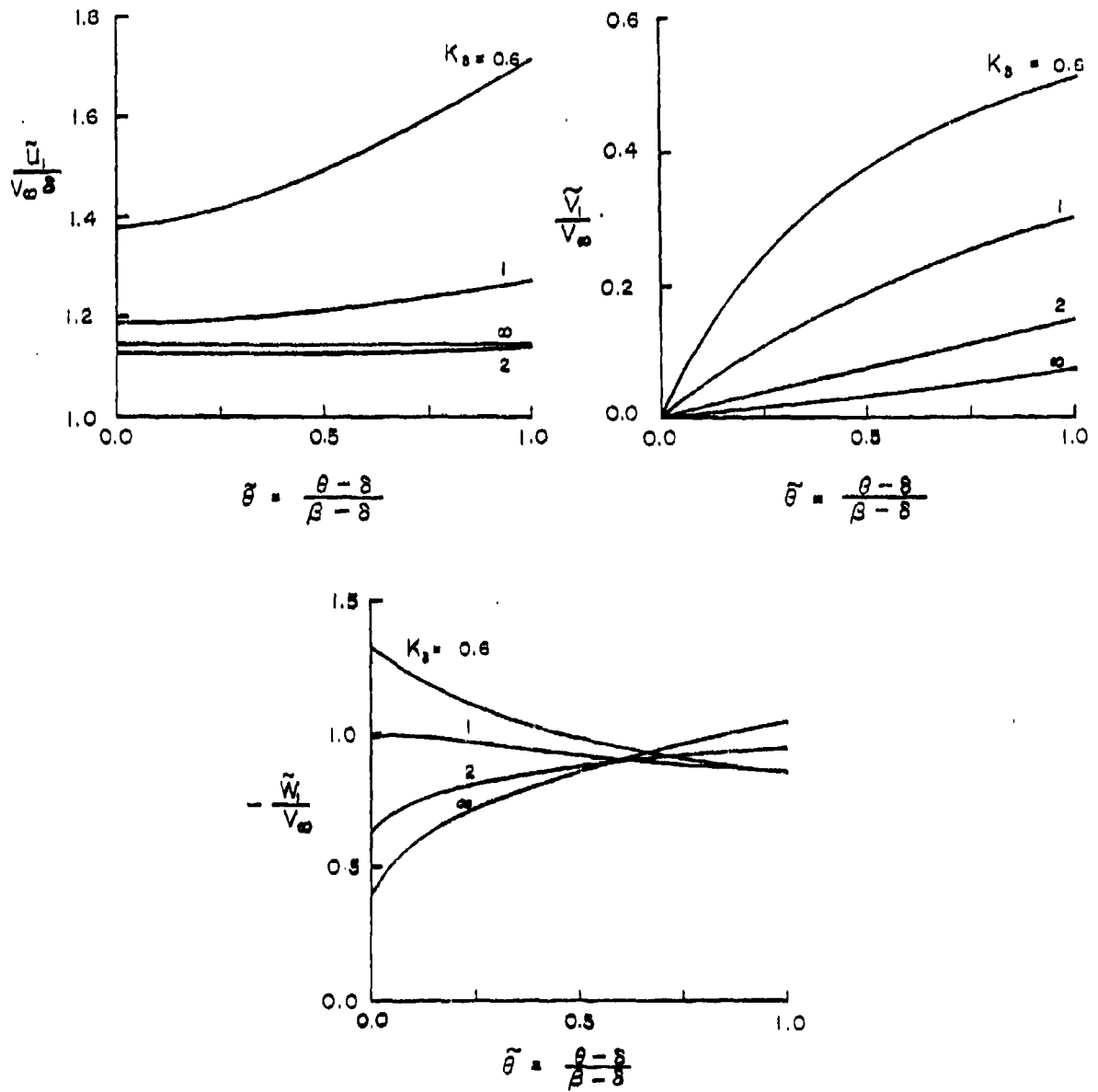


Figure 3.3 Inclined-Cone Velocity Perturbations
 a) radial
 b) polar
 c) azimuthal

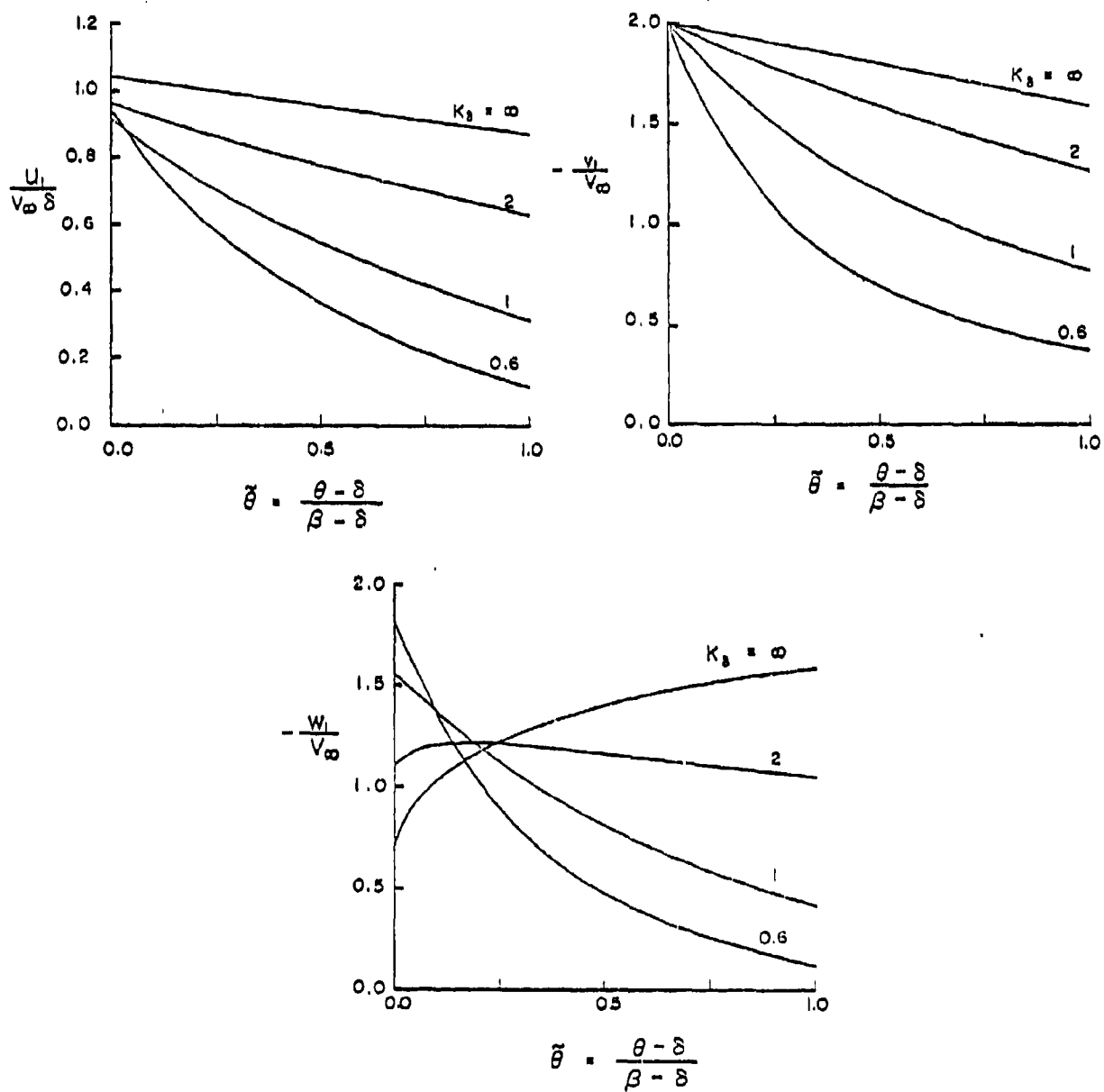


Figure 3.4 Elliptic-Cone Velocity Perturbations
 a) radial
 b) polar
 c) azimuthal

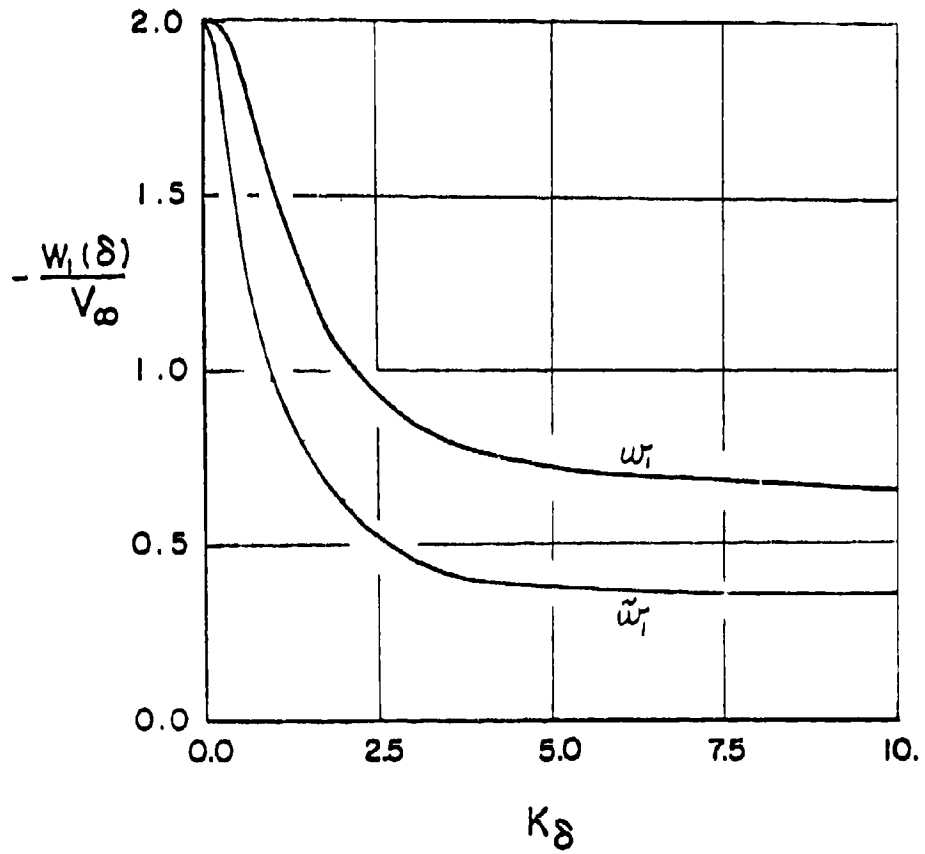


Figure 3.5 Azimuthal Velocity at the Body Surface, $\gamma = 1.4$

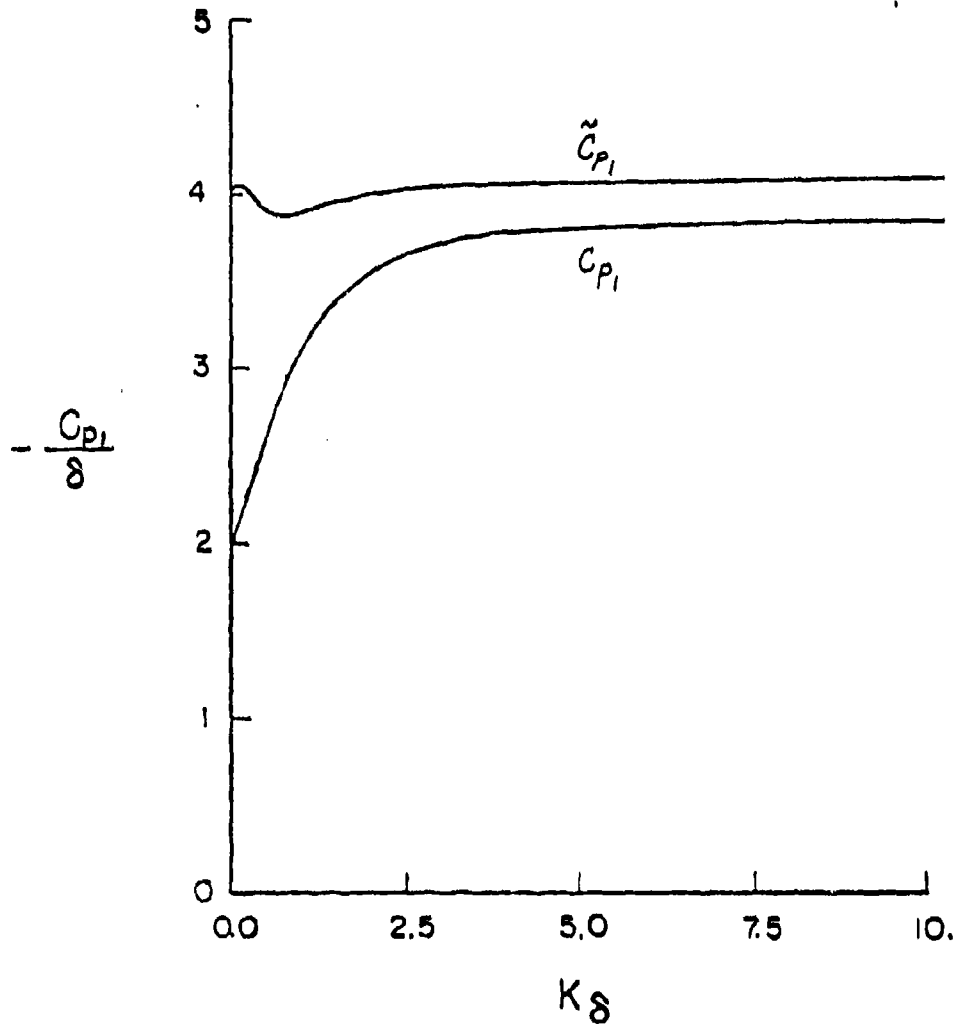


Figure 3.6 Surface Pressure Perturbations

4. Waveriders Derived from Inclined Circular Cones

4.1 Stream Surfaces

We first consider the case when $\epsilon=0$, that is, a circular cone at angle of attack. When $\epsilon=0$, we can separate the variables in Eq. (3.9), perform the integration on θ , and obtain

$$-\frac{\alpha}{V_\infty} \int_{\theta_s^*}^{\theta} \frac{\tilde{w}_1(\theta) d\theta}{\theta^2 - \delta^2} = \ln \left[\frac{\tan \frac{\phi}{2}}{\tan \frac{\phi_s}{2}} \right], \quad (4.1)$$

where

$$\theta_s^* \equiv \beta + \alpha \tilde{g} \cos \phi_s, \quad (4.2)$$

and ϕ_s is the azimuthal angle where the stream surface intersects the shock. The function $\tilde{w}_1(\theta)$ is known [14] and shown in Fig. 3.3c, and thus the quadrature in expression (4.1) can be evaluated numerically. When θ proceeds to the cone surface, $\theta \rightarrow \delta$, the quadrature on the left side of (4.1) diverges, and the left side tends to minus infinity. Correspondingly, the angle ϕ on the right side of (4.1) tends to zero. Thus all the stream surfaces become tangent to the body surface at $\beta=0$, the leeward ray on the cone.

4.2 Approximate Integration

Perusal of the function $\tilde{w}_1(\theta)$ in Fig. 3.3c suggests that \tilde{w}_1 can be approximated by the relation

$$\tilde{w}_1(\theta) = A + \frac{\delta B}{\theta}, \quad (4.3a)$$

$$\text{where } A \equiv \frac{\tau \tilde{w}_1(\beta) - \tilde{w}_1(\delta)}{\tau - 1}, \quad (4.3b)$$

$$B \equiv \frac{\tau [\tilde{w}_1(\delta) - \tilde{w}_1(\beta)]}{\tau - 1}, \quad (4.3c)$$

and $\tau \equiv \beta/\delta$. When this approximation is substituted into the integral in

Eq. (4.1) and the integral evaluated, we obtain

$$\tilde{k}_1 \ln \left[\frac{\Theta - \delta}{\Theta_s^* - \delta} \right] + \tilde{k}_2 \ln \left[\frac{\Theta + \delta}{\Theta_s^* + \delta} \right] - (\tilde{k}_1 + \tilde{k}_2) \ln \left[\frac{\Theta}{\Theta_s^*} \right] = \ln \left[\frac{\tan \frac{\phi}{2}}{\tan \frac{\phi_s}{2}} \right], \quad (4.4)$$

where
$$\tilde{k}_1 \equiv -\frac{1}{2} \frac{\alpha}{\delta} \frac{\tilde{W}_1(\delta)}{V_\infty}, \quad (4.5a)$$

$$\tilde{k}_2 \equiv -\frac{\alpha}{\delta} \frac{(\sigma+1)\tilde{W}_1(\delta) - 2\sigma\tilde{W}_1(\beta)}{2(\sigma-1)V_\infty}. \quad (4.5b)$$

Equation (4.4) can also be written as

$$\left[\frac{\Theta - \delta}{\Theta_s^* - \delta} \cdot \frac{\Theta_s^*}{\Theta} \right]^{\tilde{k}_1} \left[\frac{\Theta + \delta}{\Theta_s^* + \delta} \cdot \frac{\Theta_s^*}{\Theta} \right]^{\tilde{k}_2} = \frac{\tan \frac{\phi}{2}}{\tan \frac{\phi_s}{2}} \quad (4.6)$$

Expression (4.6) gives a relation between Θ/δ and ϕ , with ϕ_s , α/δ , and K_s as parameters. (Recall that $\sigma \equiv \beta/\delta$ is given by Eq. (3.5).) The parameter \tilde{k}_1 is always positive since $\tilde{W}_1(\delta)$ is negative when α is positive, and vice versa. The dependency of \tilde{k}_1 on K_s can be determined with the aid of Fig. 3.4. The parameter \tilde{k}_2 changes sign as K_s varies, as might be anticipated from perusal of Fig. 3.3c. It can be shown that [11,12]

$$\frac{\tilde{W}_1(\beta)}{V_\infty} = -(\sigma^2 - \tilde{g})/\sigma^2. \quad (4.7)$$

We can thus write \tilde{k}_2 as

$$\tilde{k}_2 = -\frac{\alpha}{\delta} \frac{\sigma^2(\sigma+1) \left\{ \frac{\tilde{W}_1(\delta)}{V_\infty} \right\} + 2\sigma(\sigma^2 - \tilde{g})}{2\sigma^2(\sigma-1)}. \quad (4.8a)$$

The dependency of \tilde{k}_2 on K_s is shown in Fig. 4.1. At $K_s = 0$ and $K_s = 0.9$, the parameter \tilde{k}_2 is zero. It is positive when $0 < K_s < 0.9$ and negative when $K_s > 0.9$.

Several typical stream surfaces (plotted as $Z \tan \Theta$ vs. Θ , with $Z = \text{constant}$ and $\tan \Theta = \Theta$, that is, projections on a plane perpendicular to the cone axis) are shown in Fig. 4.2 for $K_s = 1.3$, $\alpha/\delta = 0.2$, and $\gamma = 1.4$.

4.3 Lip Angle

We shall refer to the portion of a stream surface adjacent to the shock as the lip of the stream surface. The acute angle between the lip of a stream surface and the plane surface passing through the lip and the axis of the body cone is referred to as the lip angle, denoted by $\tilde{\lambda}$. If $\phi = \phi(\Theta)$ denotes the functional form for a stream surface, then the unit normal vector to a stream surface is given by

$$\hat{n} = \frac{\hat{e}_\phi - \sin \Theta \frac{d\phi}{d\Theta} \hat{e}_\Theta}{[1 + \sin^2 \Theta \left(\frac{d\phi}{d\Theta}\right)^2]^{1/2}}, \quad (4.9)$$

where \hat{e}_ϕ and \hat{e}_Θ are the azimuthal and polar spherical unit basis vectors.

The lip angle is determined by $\cos \tilde{\lambda} = \hat{e}_\phi \cdot \hat{n}$, and we find that, for small angles Θ ,

$$\tan \tilde{\lambda} = \Theta_s^* \left(\frac{d\phi}{d\Theta}\right)_s. \quad (4.10)$$

From Eq. (3.9) we determine that

$$\Theta_s^* \left(\frac{d\phi}{d\Theta}\right)_s = \frac{\alpha w_1(\beta) \sin \phi_s}{v_0(\beta)} = -\frac{\alpha}{\delta} \frac{\tilde{w}_1(\beta)}{V_\infty} \frac{\sigma \sin \phi_s}{\sigma^2 - 1}. \quad (4.11)$$

Utilizing Eq. (4.7) we determine the lip angle to be

$$\tan \tilde{\lambda} = \frac{\alpha}{\delta} \frac{\sigma^2 - \tilde{q}}{\sigma^2 - 1} \sin \phi_s. \quad (4.12)$$

The dependency of $\tilde{\lambda}$ on K_s is shown in Fig. 4.3. The ratio $(\tan \tilde{\lambda}) \csc^2 \phi_s / (\alpha/\delta)$ increases from zero to the asymptotic value 5.5 as K_s increases from zero to infinity. The lip angle thus becomes thicker as α/δ and K_s increase separately, and it is a maximum when $\phi_s = 90^\circ$.

4.4 Spacing of the Stream Surfaces

In Eqs. (4.1) or (4.6), the value of ϕ_s designates a particular stream surface, and a stream surface can be represented functionally by $\phi_s = \phi_s(\theta, \phi) = \text{constant}$. How closely the stream surfaces are spaced as θ is varied outward from the cone surface, for a fixed azimuthal angle ϕ , can be evaluated by the derivative $(\partial\phi_s/\partial\theta)$ with ϕ held constant. From Eq. (4.1) we obtain

$$\begin{aligned} \left(\frac{\partial\phi_s}{\partial\theta}\right)_\phi &= -\frac{\alpha\hat{W}_1(\theta)\sin\phi}{\partial V_\sigma(\theta)} \quad , \\ &= \frac{\alpha}{\delta} \frac{\hat{W}_1(\theta)}{V_\infty} \frac{\sin\phi}{\theta^2 - \delta^2} \quad . \end{aligned} \quad (4.13)$$

In terms of the normalized shock-layer variable $\tilde{\theta}$ defined by expression (3.7), we have

$$\left(\frac{\partial\phi_s}{\partial\tilde{\theta}}\right)_\phi = \frac{\alpha}{\delta} \frac{\hat{W}_1(\tilde{\theta}, K_\delta)}{V_\infty} \frac{\sin\phi}{\tilde{\theta}[2+(\sigma-1)\tilde{\theta}]} \quad . \quad (4.14)$$

This derivative increases when x increases and goes to infinity when $\tilde{\theta}$ goes to zero ($\theta \rightarrow \delta$), and the stream surfaces become more closely spaced correspondingly. As seen from Fig. 3.3c, the derivative is insensitive to variations in K_δ when $\tilde{\theta}$ is about 0.7. When $\tilde{\theta}$ is less than 0.7, the derivative decreases as K_δ increases, and vice versa when $\tilde{\theta}$ is greater than 0.7, but to a lesser degree.

4.5 Waveriders with a Freestream Upper Surface

Any stream surface just described can be utilized as a solid surface, but a complementary surface remains to be described in order to fashion a closed aerodynamic body. In this section we choose such surfaces that are parallel to the free stream. We first demarcate the axis passing through the vertex that is aligned with the free stream. This axis is inclined by an angle α with the cone axis. Any plane passing through this freestream axis is parallel to the free stream. We select pairs of these freestream planes that pass through the lipshock intersection of the conical stream surfaces, and a closed aerodynamic body is thus formed. The upper surfaces are pairs of freestream planes passing through the freestream vertex axis, and the lower surface is a stream surface of the inclined circular-cone flow field. These surfaces join together at the lip-shock intersection. An example is shown in Fig. 4.4 for which the lip-shock intersection occurs at $\phi_s = 90^\circ$.

There are an infinite number of such aerodynamic waveriders, depending on how the freestream planes are selected. As a step towards distinguishing between the different configurations, let us determine the lip angle, χ_w , between the freestream planes and the conical stream surfaces. The normal unit vector to a freestream plane intersecting the shock at ϕ_s is, for small angles

$$\hat{n}_\infty = \frac{[\sigma - (\frac{\alpha}{\beta})(1-\tilde{q}) \cos \phi_s] \hat{e}_\phi - (\frac{\alpha}{\beta}) \sin \phi_s \hat{e}_\theta}{\sqrt{[\sigma - (\frac{\alpha}{\beta})(1-\tilde{q}) \cos \phi_s]^2 + (\frac{\alpha}{\beta})^2 \sin^2 \phi_s}} \quad (4.15)$$

The lip angle, $\tilde{\lambda}_W$, is determined by the condition

$$\cos \tilde{\lambda}_W = \hat{n}_\infty \cdot \hat{n} \quad , \quad (4.16)$$

where \hat{n} is the unit normal vector of the conical stream surface evaluated at the shock, given by Eq. (4.9). We find for small ratios $\alpha/\delta \ll 1$ that

$$\tan \tilde{\lambda}_W \approx \frac{\alpha}{\delta} \left[\frac{\sigma^2 - \tilde{g}}{\sigma(\sigma^2 - 1)} - \frac{1}{\sigma - \frac{\alpha}{\delta} (1 - \tilde{g}) \cos \phi_S} \right] \sin \phi_S \quad . \quad (4.17)$$

If the waverider lip angle is ever to be a cusp, then we must have $\tilde{\lambda}_W = 0$. The right side of Eq. (4.17) can vanish only when $\sin \phi_S = 0$ or when

$$\frac{\alpha}{\delta} \cos \phi_S = \frac{\sigma}{\sigma^2 - \tilde{g}} \quad . \quad (4.18)$$

The right-hand side of Eq. (4.18) vanishes when $K_\delta \rightarrow 0$ and increases to 0.87 when $K_\delta \rightarrow \infty$. When $K_\delta = 0.5$ and $\alpha/\delta = 0.5$, then Eq. (4.18) yields $\phi_S = 0$, and a cusp can occur only at $\phi_S = 0$. When K_δ is larger than 0.5 and α/δ is less than 0.5 a cusp cannot occur except at $\phi_S = 0^\circ$ or 180° . These are generally the conditions of interest and, as such, the possibility of a cusp is of no concern.

From structural or heating considerations, the condition where the lip angle $\tilde{\lambda}_W$ is a maximum is of interest. Setting the derivative of $\tilde{\lambda}_W$ with respect to ϕ_S equal to zero yields, for small α/δ ,

$$\cos \phi_S = - \frac{\sigma^2 - 1}{\sigma} \frac{\alpha}{\delta} \quad . \quad (4.19)$$

When the right-hand side is less than minus unity, no relative maximum occurs.

When the right-hand side is small, we obtain

$$\phi_s \approx \frac{\pi}{2} + \frac{\sigma^2 - 1}{\sigma} \frac{\alpha}{\delta} \quad (4.20)$$

which illustrates that the maximum value of λ_w occurs when $\phi_s > \pi/2$. When $K_\delta = 1.3$, $\gamma = 1.4$, and $\alpha/\delta = 0.2$, $\lambda_w = 8.6^\circ$ is a maximum when $\phi_s = 96.8^\circ$. This particular waverider is similar in shape to that shown in Fig. 4.4, for which $\phi_s = 90^\circ$ and $\lambda_w = 8.57^\circ$. The upper surfaces in these cases appear to have a positive dihedral angle.

Another waverider can be formed in which the two upper freestream planes are parallel, that is, the upper surface is flat. An example is shown in Fig. 4.5. From geometrical considerations, this situation occurs when, for small α/δ ,

$$\cos \phi_s = \frac{(\alpha/\delta)}{\sigma} \quad (4.21)$$

For $K_\delta = 1.3$, $\gamma = 1.4$, and $\alpha/\delta = 0.2$, we get $\phi_s = 81.4^\circ$ and $\lambda_w = 8.2^\circ$. This waverider is akin to the waverider formed from a half cone at zero angle of attack with a symmetry plane through the cone axis identified as a flat, zero-thickness delta wing. The waverider shown in Fig. 4.5, however, while having a flat upper surface, has a faired under surface with a "wing" of finite thickness. This waverider can be said to have zero dihedral angle.

Other waveriders in this family can be formed that have negative dihedral angles. These exist when ϕ_s is less than the value given by Eq. (4.21). An example is shown in Fig. 4.6 for $\phi_s = 70^\circ$ and $\lambda_w = 7.6^\circ$. All of the waveriders in this section are lifting bodies since the lower conical surface is at a higher pressure than the upper freestream surfaces.

4.6 Waveriders with a Complementary Wedge Surface

Another means of deriving a closed aerodynamic shape in conjunction with a conical stream surface is to use plane surfaces passing through the cone axis. In these cases the freestream flow must be deflected by the angle α . We can thus use the formulas for the fundamental wedge-derived waverider obtained in Section 1, setting $\Delta = \alpha$. Let the angle between the two cone-axis plane surfaces be denoted by 2ψ , where ψ is the dihedral angle, as shown in Fig. 4.7. The plane (or wedge) shock wave across the top of the waverider is oriented at an angle β_W with the free stream, and it is related to the cone shock by the relation

$$\begin{aligned} \beta_W - \alpha &= \phi_S^* \cos \psi \\ &= (\beta + \alpha \gamma \cos \phi_S) \cos \psi \end{aligned} \quad (4.22)$$

We now note that $\phi_S = \pi - \psi$ and that β_W is given by Eq. (2.1), with $\sin \beta = \beta_W$ and $\sin \Delta = \alpha$. We thus rewrite Eq. (4.24) as

$$\frac{\alpha}{\delta} \left[\frac{\gamma+1}{4} + \sqrt{\left(\frac{\gamma+1}{4}\right)^2 + \frac{1}{K_\delta^2} \left(\frac{\delta}{\alpha}\right)^2} \right] = \left[\frac{\beta}{\delta} - \frac{\alpha}{\delta} \gamma \cos \psi \right] \cos \psi \quad (4.23)$$

Recalling that $\sigma \equiv \beta/\delta$ is given by Eq. (3.5), we note that Eq. (4.25) provides a relation between α/δ , K_δ , and ψ . Solving for α/δ , we obtain

$$\frac{\alpha}{\delta} = \frac{B \sigma \cos \psi \pm \sqrt{\left(\frac{\gamma+1}{4} \sigma \cos \psi\right)^2 - \frac{1}{K_\delta^2} \left\{ \left(\frac{\gamma+1}{4}\right)^2 - B^2 \right\}}}{\left(\frac{\gamma+1}{4}\right)^2 - B^2} \quad (4.24)$$

where

$$B \equiv \frac{3-\gamma}{4} - \gamma \cos \psi \quad (4.25)$$

Figure 4.8 shows α/δ plotted as a function of K_δ for various values of the dihedral angle ψ and for $\gamma = 1.4$. We observe that α/δ is double valued for fixed values of K_δ and ψ , but this is only apparent for $\psi > 75^\circ$ since the curves are plotted for only the realistic values of $\alpha/\delta < 1$. The condition $\alpha/\delta = 0$ corresponds to zero flow deflection over the upper surface; the dihedral angle ψ is such that a plane Mach surface sits on the lip of the waverider, and the lips extend to the cone surface as a pair of infinitesimally thin delta wings.

The lift on the waveriders in this section may be positive or negative depending on the value of α/δ . The pressure in the conical flow field is given by

$$\frac{C_{p_c}(\theta, \phi)}{\delta^2} = \frac{C_{p_o}(\theta)}{\delta^2} + \frac{\alpha}{\delta} \frac{C_{p_1}(\theta)}{\delta} \cos \phi + O(\alpha^2) \quad , \quad (4.26)$$

and the pressure in the wedge flow field is given by (from Eq. (2.2))

$$\frac{C_{p_w}}{\delta^2} = \frac{\gamma+1}{2} \left(\frac{\alpha}{\delta}\right)^2 + \sqrt{\left(\frac{\gamma+1}{2}\right)^2 \left(\frac{\alpha}{\delta}\right)^4 + \frac{4}{K_\delta^2} \left(\frac{\alpha}{\delta}\right)^2} \quad . \quad (4.27)$$

The minimum pressure on the conical stream surface occurs at the symmetry plane, $\theta = \delta$ and $\phi = 0$. The minimum lifting pressure differential is thus given by

$$\frac{\Delta C_{p_m}}{\delta^2} = \frac{C_{p_c}(\delta, 0)}{\delta^2} - \frac{C_{p_w}}{\delta^2} \quad (4.28)$$

We also note that [, ,]

$$\frac{C_{p_o}(\delta)}{\delta^2} = 1 + \frac{\sigma^2 \ln \sigma^2}{\sigma^2 - 1} \quad (4.29)$$

Further, from Fig. 3.6, we note the $\tilde{C}_{p1}(\delta)/\delta \approx -4$. A lower bound for the value of α/δ corresponding to zero lift can now be found by setting $\Delta C_{pm} = 0$:

$$1 + \frac{\alpha^2 \ln \sigma^2}{\sigma^2 - 1} - 4\left(\frac{\alpha}{\delta}\right) - \frac{\gamma+1}{2} \left(\frac{\alpha}{\delta}\right)^2 - \sqrt{\left(\frac{\gamma+1}{2}\right)^2 \left(\frac{\alpha}{\delta}\right)^4 + \frac{4}{K_\delta^2} \left(\frac{\alpha}{\delta}\right)^2} = 0 \quad (4.30)$$

This relation provides α/δ for zero lift as a function of K_δ and is shown in Fig. 4.7. The waveriders described by conditions below this line are lifting when the conical surface is underneath, and the waveriders described by conditions above the line are lifting when the wedge surface is underneath.

Approximately, the zero lift conditions occur when $\alpha/\delta \approx 0.4$ for $K_\delta > 1$.

A systematic variation of the cone-wedge waverider cross section geometries is shown in Figs. 4.9a, b, c, d, e, f for $\alpha/\delta = 0.1, 0.2, 0.3, 0.4, 0.5, 0.6$. For each value of α/δ , dihedral angles of $\psi = 45^\circ, 60^\circ, 70^\circ, 75^\circ, 80^\circ$ are shown along with their corresponding values of K_δ as determined from Eqs. (4.25) or (4.26). For $\alpha/\delta = 0.1, 0.2$, and 0.3 , the bodies are lifting when the conical surface is underneath. At $\alpha/\delta = 0.4$, the body is nearly at zero lift. For $\alpha/\delta = 0.5$ and 0.6 , the bodies are lifting when the wedge surface is underneath. The shock lies closer to the body when K_δ is larger, and hence when ψ is larger. The standard conditions $K_\delta = 1.3$, $\gamma = 1.4$, and $\alpha/\delta = 0.2$ are represented in Fig. 4.7, in which case $\psi = 57^\circ$ and $\lambda = 15^\circ$.

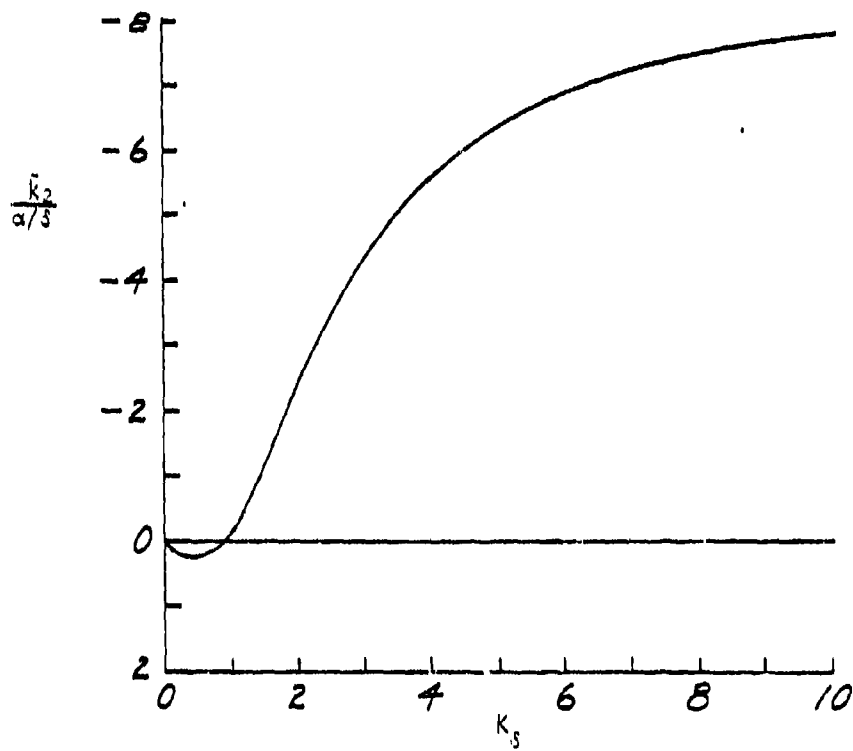


Figure 4.1 Circular-Cone Stream-Surface Function

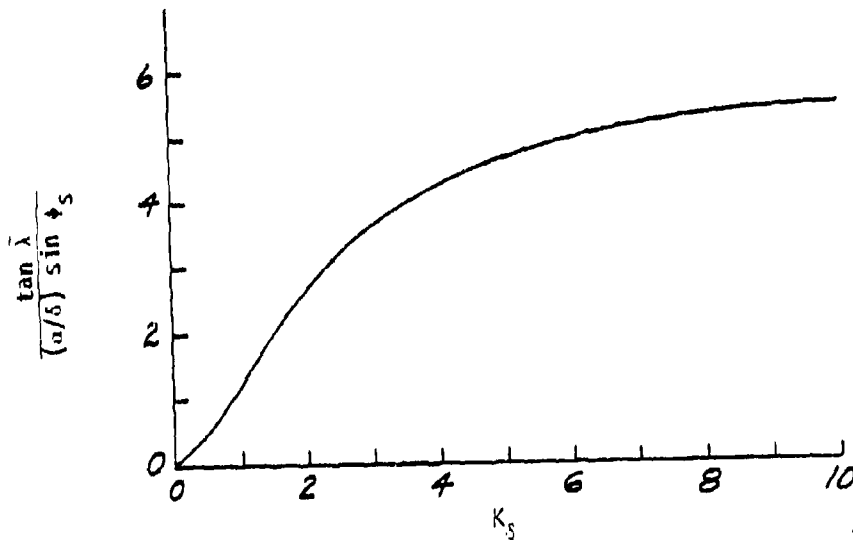
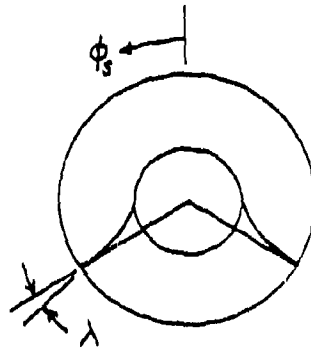


Figure 4.2 Circular-Cone Lip Angle

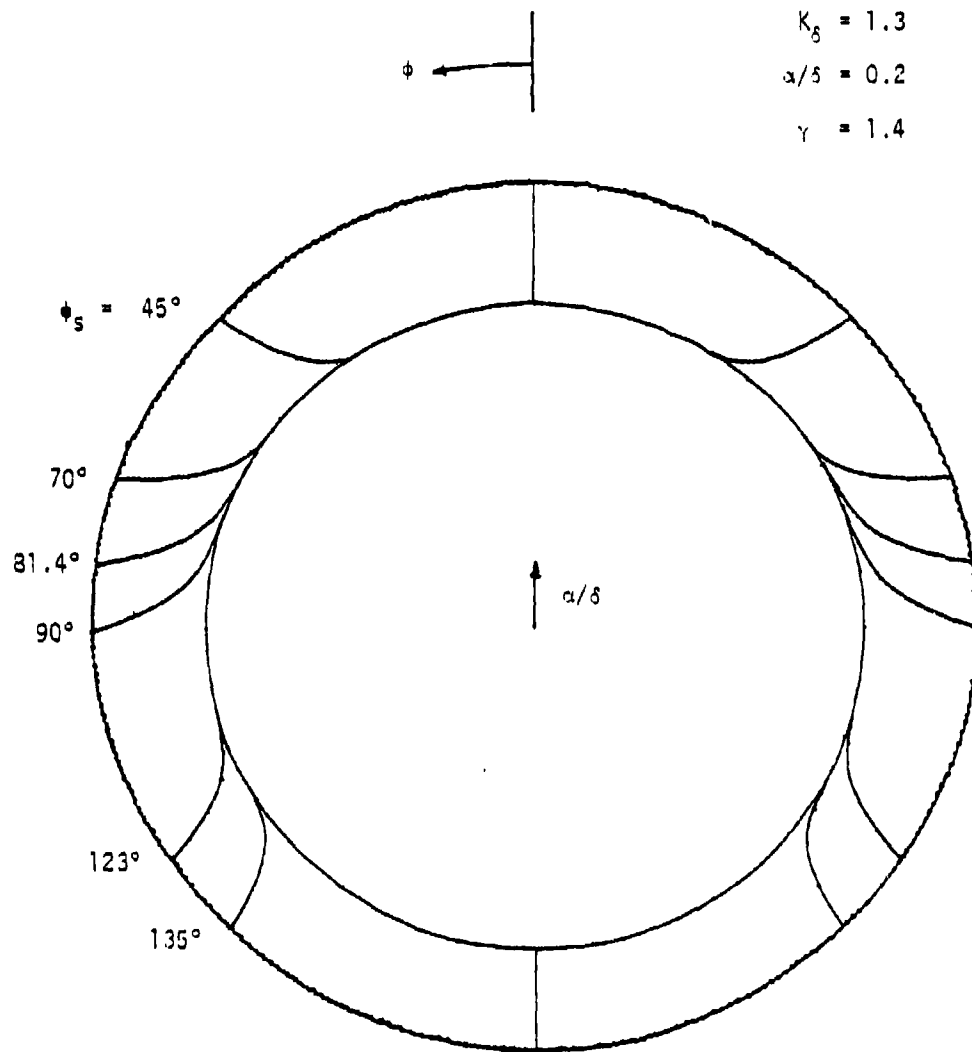


Figure 4.3 Stream Surfaces For Inclined Cone

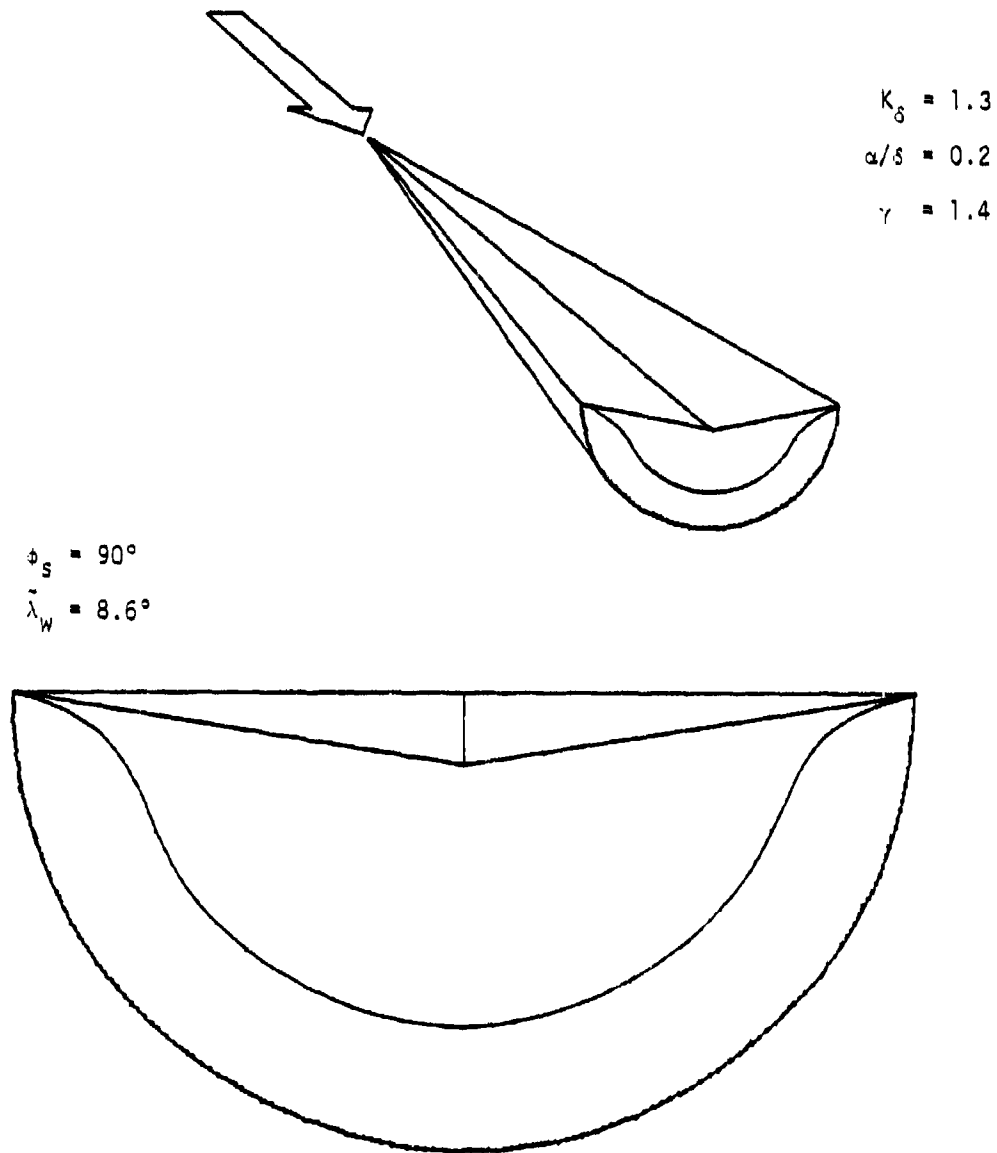


Figure 4.4 Circular-Cone Waverider With Freestream Upper Surface: Positive Dihedral

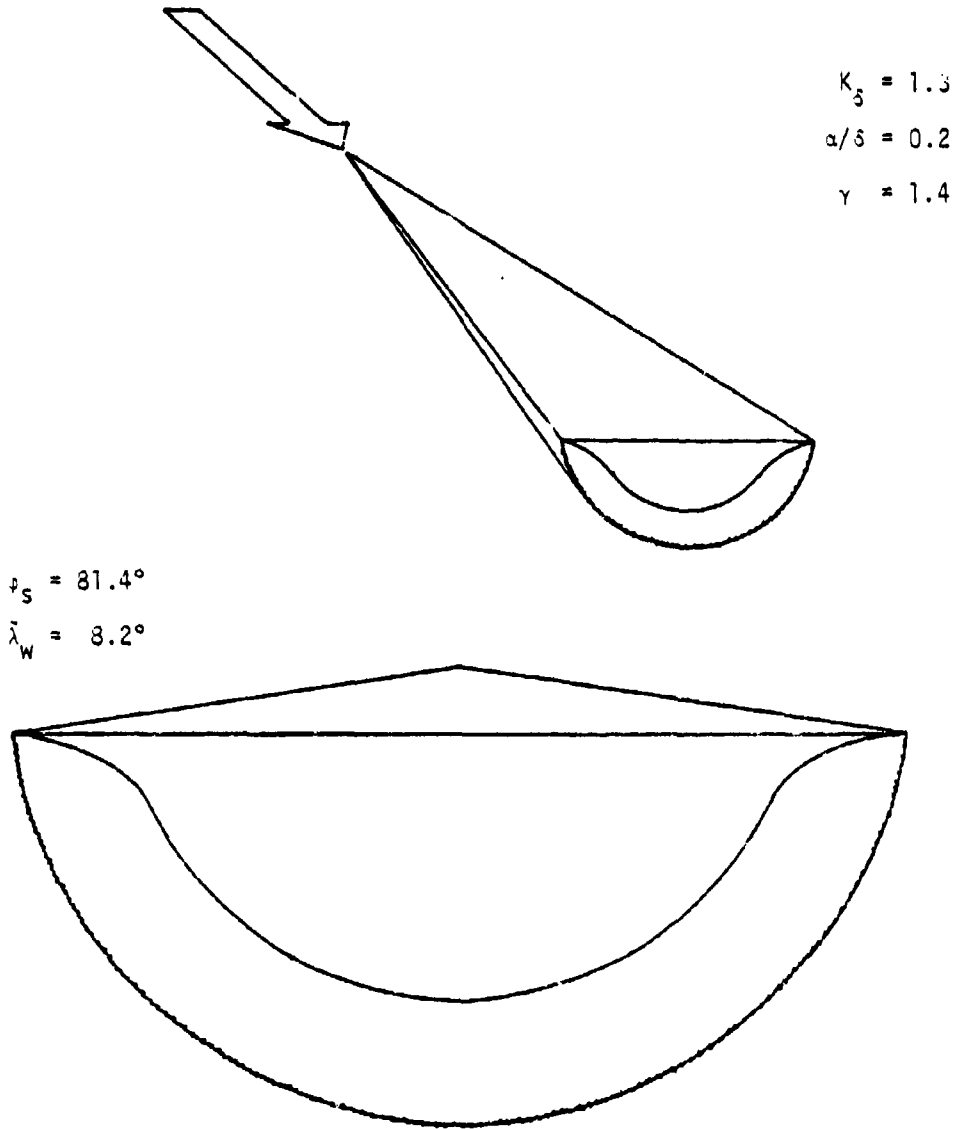


Figure 4.5 Circular-Cone Waverider With Freestream Upper Surface: Zero Dihedral

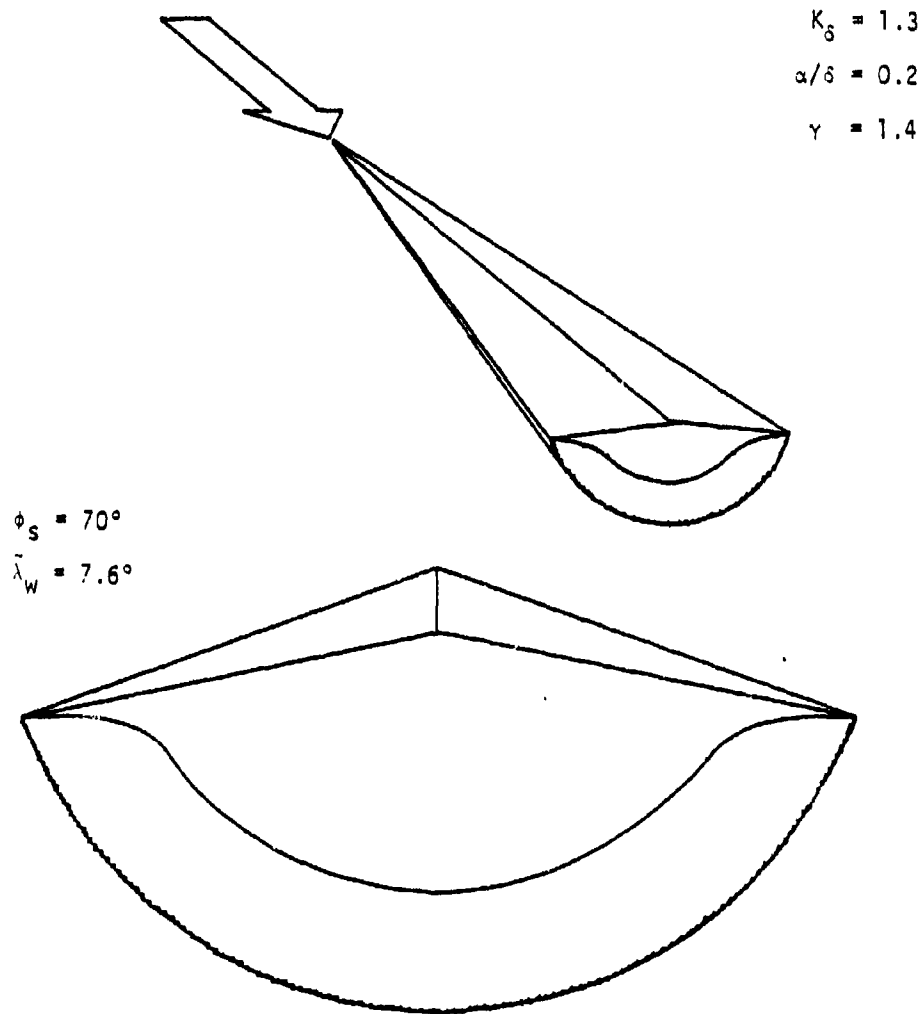


Figure 4.6 Circular-Cone Waverider With Freestream Upper Surface: Negative Dihedral

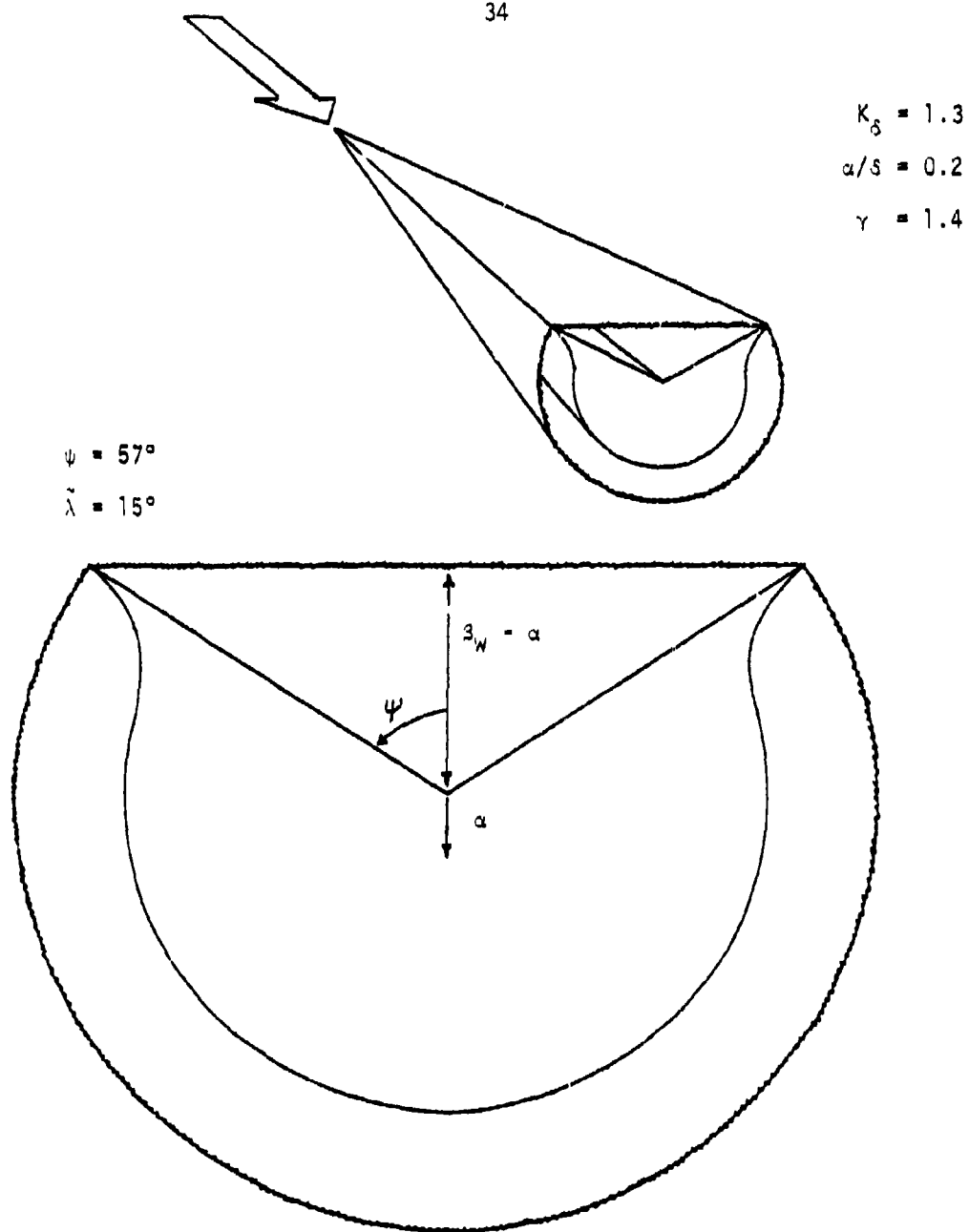


Figure 4.7 Circular-Cone Waverider With Wedge-Shock Upper Surface

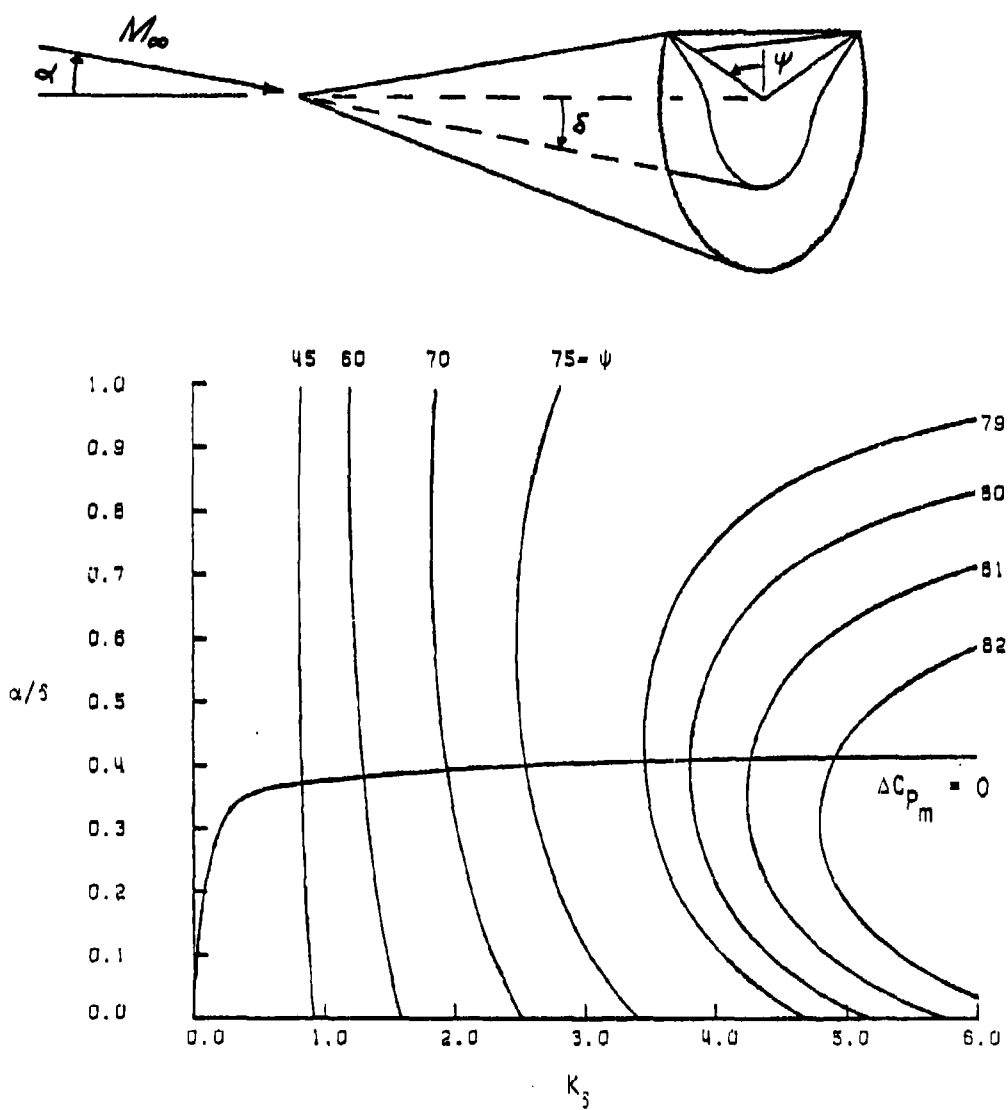


Figure 4.8 α/δ Versus K_3 For Various Dihedral Angles

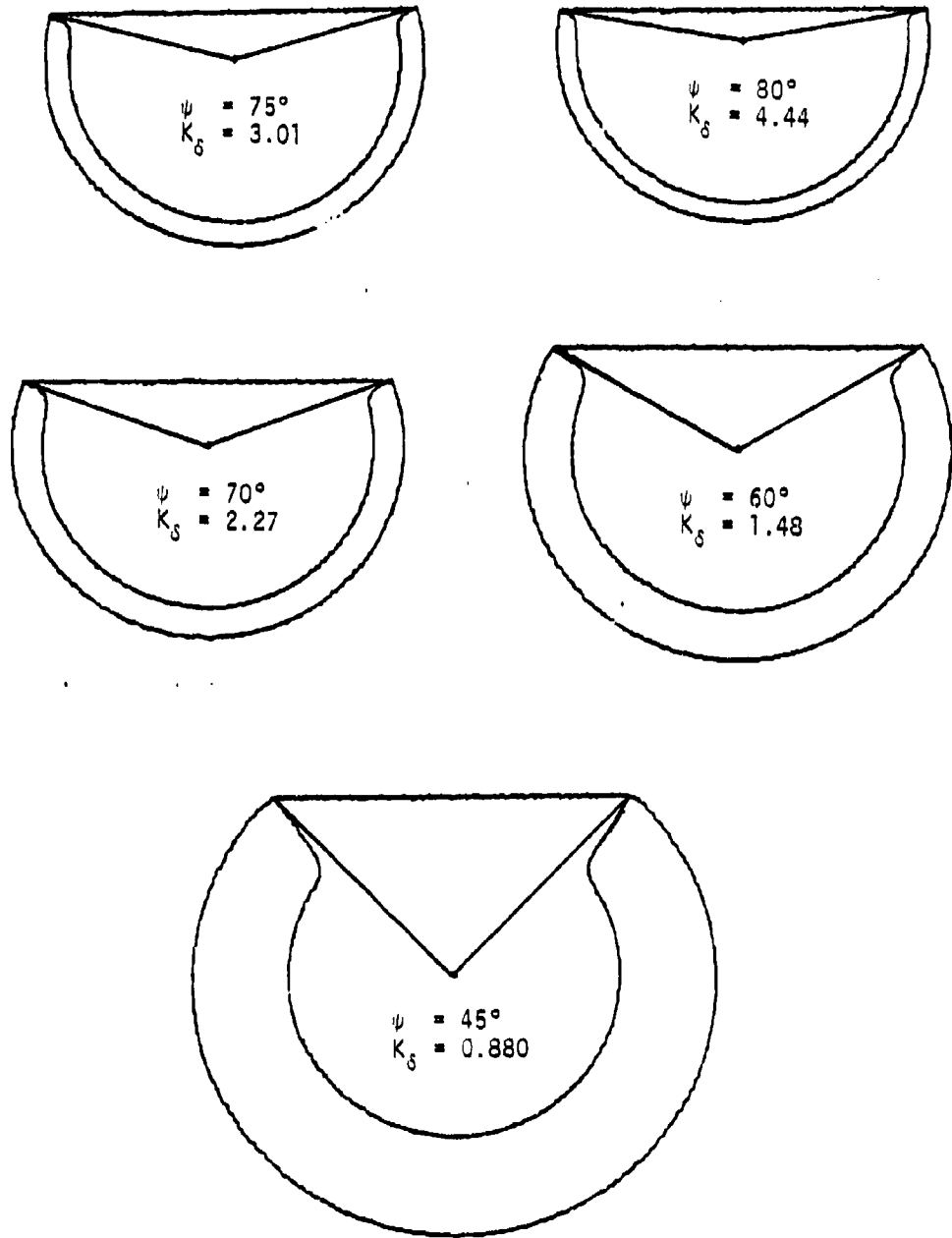


Figure 4.9a Wedge Shock-Circular Cone Waveriders,
 $\alpha/\beta = 0.1$

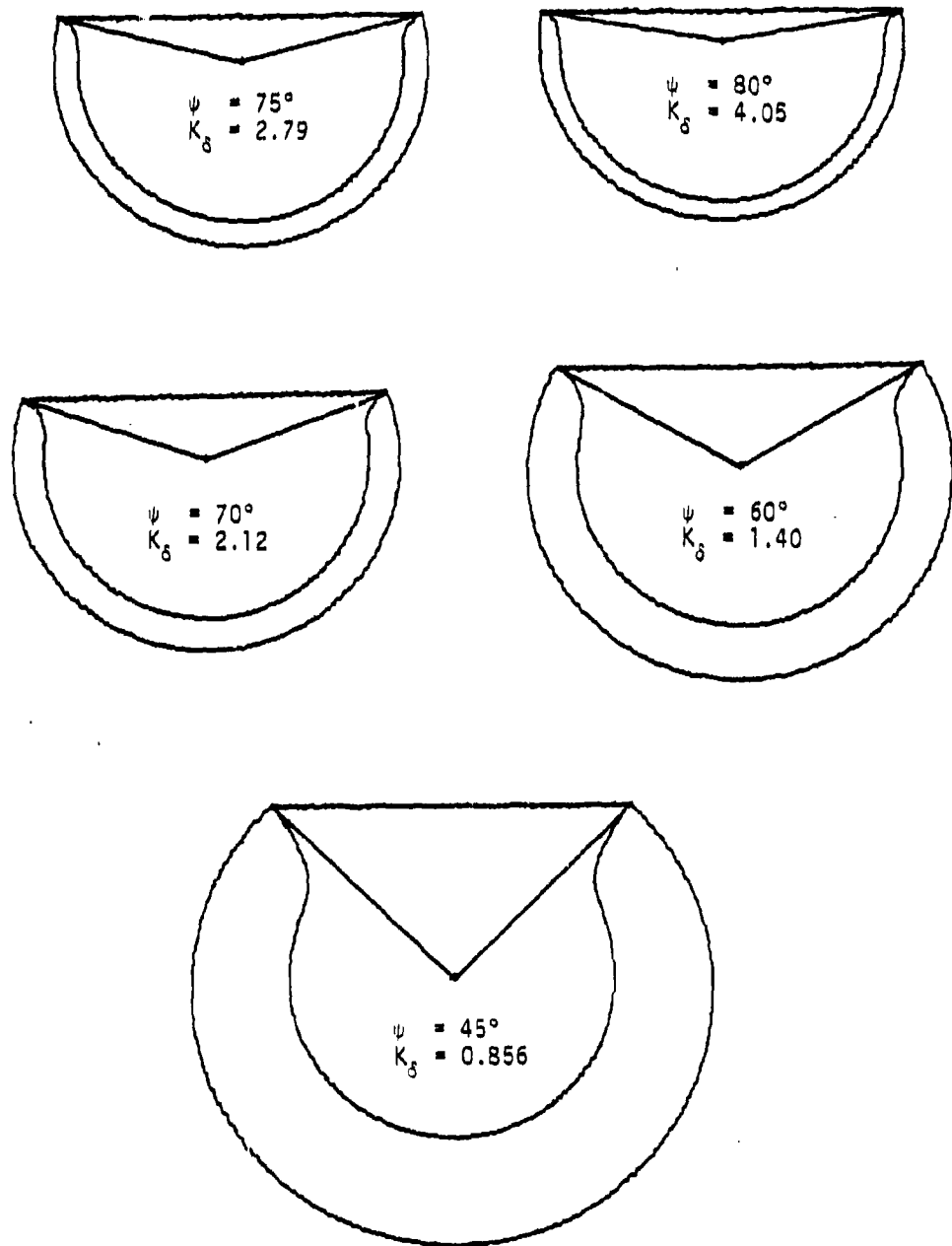


Figure 4.9b Wedge Shock-Circular Cone Waveriders,
 $\alpha/s = 0.2$

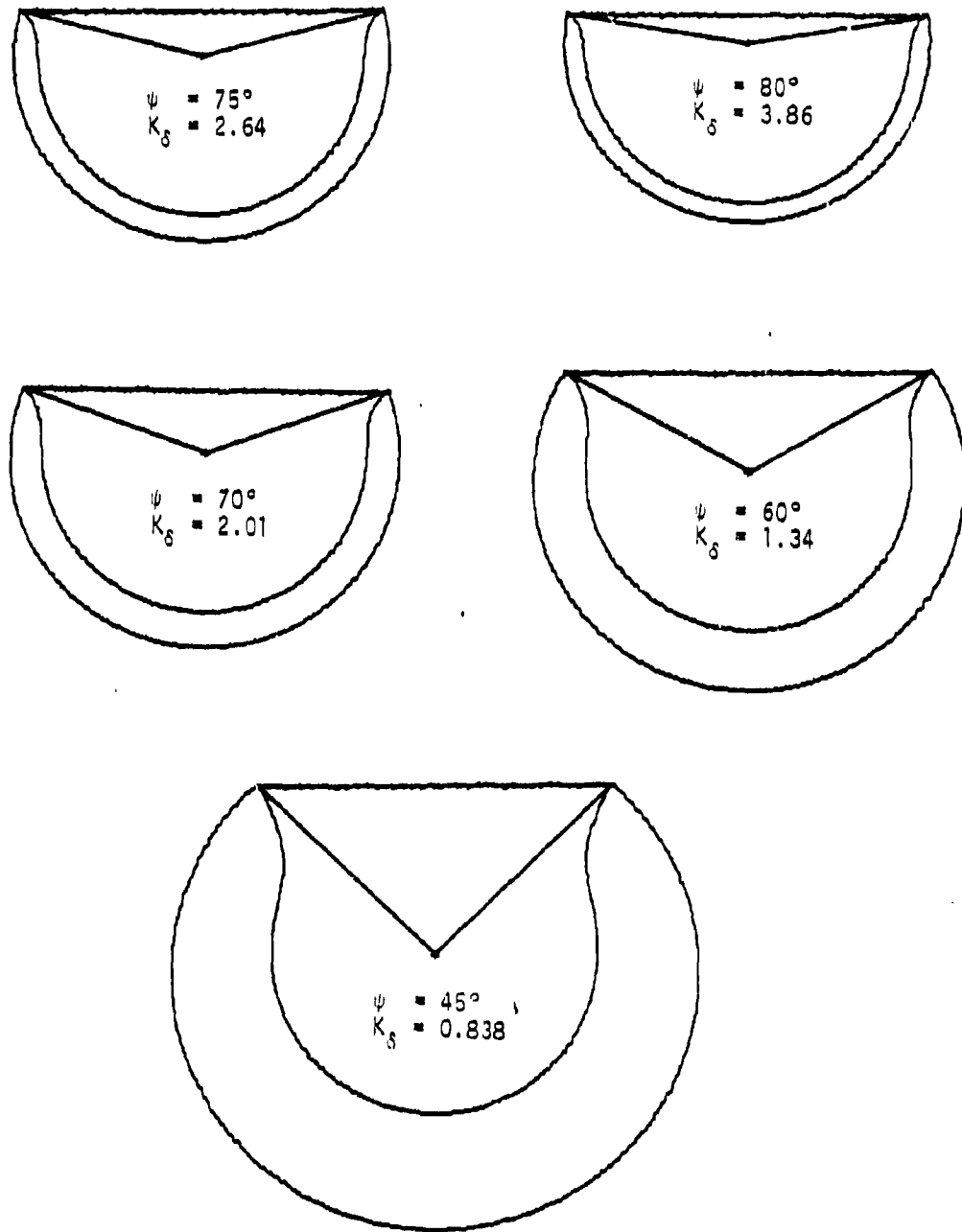


Figure 4.9c Wedge Shock-Circular Cone Waveriders,
 $\alpha/\delta = 0.3$

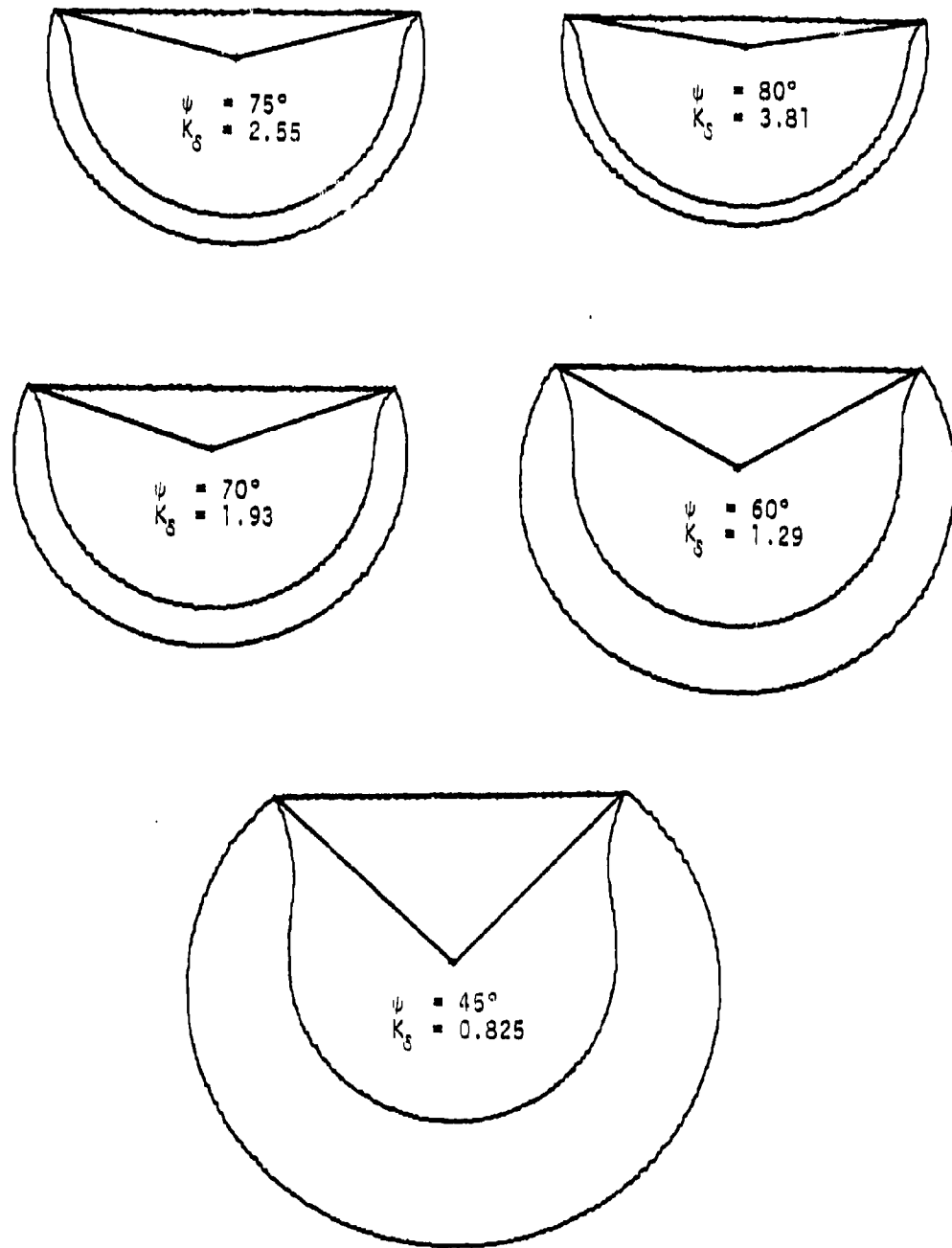


Figure 4.9d Wedge Shock-Circular Cone Waveriders,
 $\alpha/s = 0.4$

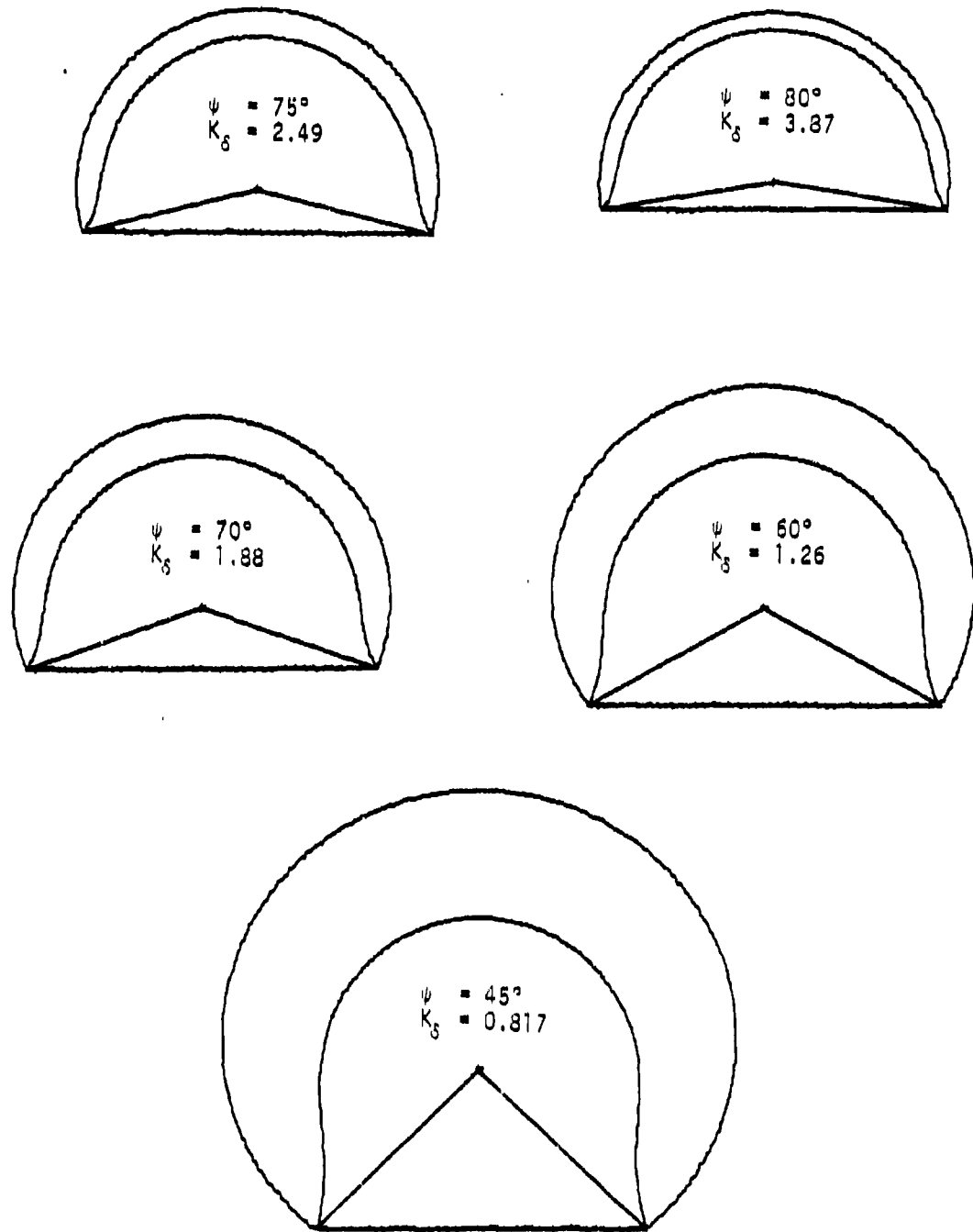


Figure 4.9e Wedge Shock-Circular Cone Waveriders,
 $x/\delta = 0.5$

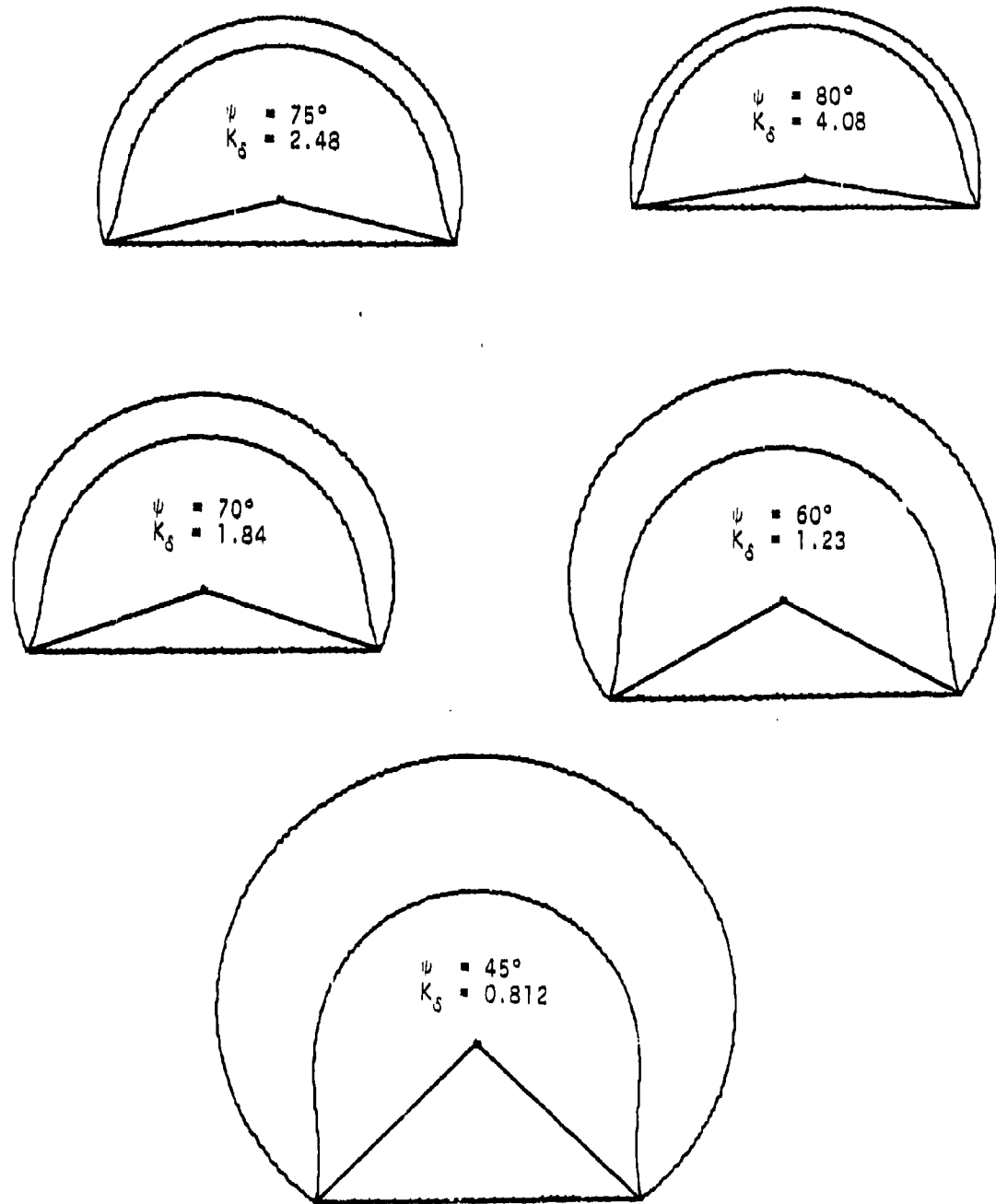


Figure 4.9f Wedge Shock-Circular Cone Waveriders,
 $u/s = 0.6$

5. Waveriders Derived from Elliptic Cones

5.1 Stream Surfaces

We now consider the case when $\alpha = 0$, that is, an elliptic cone at zero angle of attack. When $\alpha = 0$, we can separate the variables in Eq. (3.9), perform the integration on Θ , and obtain

$$-\frac{2\varepsilon}{\sqrt{\infty}} \int_{\Theta_s^*}^{\Theta} \frac{w_1(\Theta) d\Theta}{\Theta^2 - \Theta_c^2} = \ln \left[\frac{\tan \phi}{\tan \phi_s} \right] \quad , \quad (5.1)$$

where

$$\Theta_s^* \equiv \beta - \varepsilon g \cos 2\phi_s \quad , \quad (5.2)$$

and where we have replaced δ that appears in Eq. (3.10) by Θ_c , the elliptic cone angle,

$$\Theta_c \equiv \delta - \varepsilon \cos 2\phi \quad . \quad (5.3)$$

The variation of ϕ that occurs in Θ_c is to be ignored in the integration. These operations are consistent in our present first-order accuracy. The azimuthal velocity $w_1(\Theta)$ is known [13,14] and is illustrated in Fig. 3.4c. The quadrature thus can be evaluated numerically. When Θ proceeds to the cone surface, $\Theta \rightarrow \Theta_c$, the quadrature on the left side of Eq. (5.1) diverges, and the right side tends to minus infinity. Correspondingly, when the shock location of the stream surface, ϕ_s , is less than 90° , the angle ϕ tends to zero. When ϕ_s is greater than 90° , the angle ϕ tends to 180° . Thus the stream surfaces that begin at the shock for $\phi_s < 90^\circ$ become tangent to the cone surface at $\phi = 0$, and the stream surfaces that begin at the shock for $\phi_s > 90^\circ$ become tangent to the cone at $\phi = 180^\circ$. The stream surface for $\phi_s = 90^\circ$ is a symmetry plane that is perpendicular to the body at $\phi = 90^\circ$. Examples of stream surfaces are shown in Fig. 5.1.

5.2 Approximate Integration

Figure 3.4c suggests that $w_1(\theta)$ can be approximated by the relation

$$w_1(\theta) = A + \frac{\theta_c B}{\theta} \quad (5.4a)$$

where

$$A \equiv \frac{\tilde{\sigma} w_1(\theta_s) - w_1(\theta_c)}{\tilde{\sigma} - 1} \quad (5.4b)$$

$$B \equiv \frac{[w_1(\theta_c) - w_1(\theta_s)]}{\tilde{\sigma} - 1} \quad (5.4c)$$

where $\tilde{\sigma} \equiv \theta_s/\theta_c = \sigma + O(\epsilon)$, $\theta_s = \beta + O(\epsilon)$, and $\theta_c = \delta + O(\epsilon)$. The errors of order ϵ in Eqs. (5.4) will subsequently be neglected. When this approximation is used to evaluate the integral in Eq. (5.1), we obtain

$$k_1 \ln \left[\frac{\theta - \theta_c}{\theta_s^* - \theta_c} \right] + k_2 \ln \left[\frac{\theta + \theta_c}{\theta_s^* + \theta_c} \right] - (k_1 + k_2) \ln \left[\frac{\theta}{\theta_s^*} \right] = \ln \left[\frac{\tan \phi}{\tan \phi_s} \right] \quad (5.5)$$

where

$$k_1 \equiv - \frac{\epsilon}{\delta} \frac{w_1(\delta)}{V_\infty} \quad (5.6a)$$

$$k_2 \equiv - \frac{\epsilon}{\delta} \frac{(\sigma+1) w_1(\delta) - 2\sigma w_1(\beta)}{(\sigma-1) V_\infty} \quad (5.6b)$$

Equation (5.5) can also be written as

$$\left[\frac{\theta - \theta_c}{\theta_s^* - \theta_c} \cdot \frac{\theta_s^*}{\theta} \right]^{k_1} \left[\frac{\theta + \theta_c}{\theta_s^* + \theta_c} \cdot \frac{\theta_s^*}{\theta} \right]^{k_2} = \frac{\tan \phi}{\tan \phi_s} \quad (5.7)$$

Expression (5.7) is a relation between θ/δ and ϕ_s , with ϕ_s , ϵ/δ , and K_δ as parameters. The parameter k_1 is always positive since $w_1(\delta)$ is negative when ϵ is positive, and vice versa. Figure 3.5 illustrates the dependency of k_1 on K_δ . The parameter k_2 changes sign as K_δ varies, which is suggested by the behavior of $w_1(\theta)$ shown in Fig. 3.4c. It can be shown that [13,14]

$$\frac{w_1(\beta)}{V_\infty} = - 2g/\sigma^2 \quad (5.8)$$

We can now write k_2 as

$$k_2 = -\frac{\epsilon}{\delta} \frac{4g + \sigma(\sigma+1) \{w_1(\delta)/V_\infty\}}{\sigma(\sigma-1)} \quad (5.9)$$

Figure 5.2 shows how k_2 depends on K_δ . The parameter k_2 vanishes at $K_\delta = 1.9$. In the range $0 \leq K_\delta \lesssim 1.9$, k_2 is positive, and it is negative when $K_\delta \gtrsim 1.9$.

5.3 Lip Angle

The lip angle is defined by $\cos \lambda = \hat{e}_\phi \cdot \hat{n}$, and for the elliptic conical surfaces is determined by

$$\begin{aligned} \tan \lambda &= -\frac{\epsilon}{\delta} \frac{w_1(\delta)}{V_\infty} \frac{\sigma \sin 2\phi_S}{\sigma^2 - 1} \\ &= \frac{\epsilon}{\delta} \frac{2g \sin 2\phi_S}{\sigma(\sigma^2 - 1)} \end{aligned} \quad (5.10)$$

Figure 5.3 shows the dependency of λ on K_δ . The ratio $(\tan \lambda)(\csc 2\phi_S)/(\epsilon/\delta)$ increases from zero to the asymptotic value 8.7 as K_δ increases from zero to infinity. The lip angle becomes thicker as K_δ and ϵ/δ increase separately. The lip angle is a maximum when $\phi_S = 45^\circ$ and 135° , and it is zero at the symmetry planes $\phi_S = 0^\circ$ and 90° .

5.4 Waveriders with a Freestream Upper Surface

The axis of the elliptic cone at zero angle of attack is parallel to the free stream, and any plane that passes through the cone axis is parallel to the free stream. We choose pairs of plane surfaces that pass through the cone axis and intersect the shock at the lips of a conical stream surface. When the plane surfaces are the upper surfaces and the conical surface is the lower surface, a lifting aerodynamic waverider is formed. Two examples are shown in Fig. 5.4 for $K_\delta = 1.3$, $\epsilon/\delta = 0.1$, and $\lambda = 1.4$. These configurations correspond to lip positions of $\phi_S = 100^\circ$ and 110° . The respective lip angles are found

to be $|\lambda| = 2.2^\circ$ and 4.0° . These elliptic-cone shapes are similar in form to the circular cone shape shown in Fig. 4.6. The elliptic cone shapes are flatter on the bottom and have thinner lip angles.

The pressure coefficient on the undersurface is given by

$$\frac{C_p(\theta, \phi)}{\delta^2} = \frac{C_{p_0}(\theta)}{\delta^2} + \left(\frac{\epsilon}{\delta}\right) \frac{C_{p_1}(\theta)}{\delta} \cos 2\phi \quad (5.11)$$

When Eq. (5.7) is used to determine θ as a function of ϕ , the surface pressure as a function of ϕ can be determined.

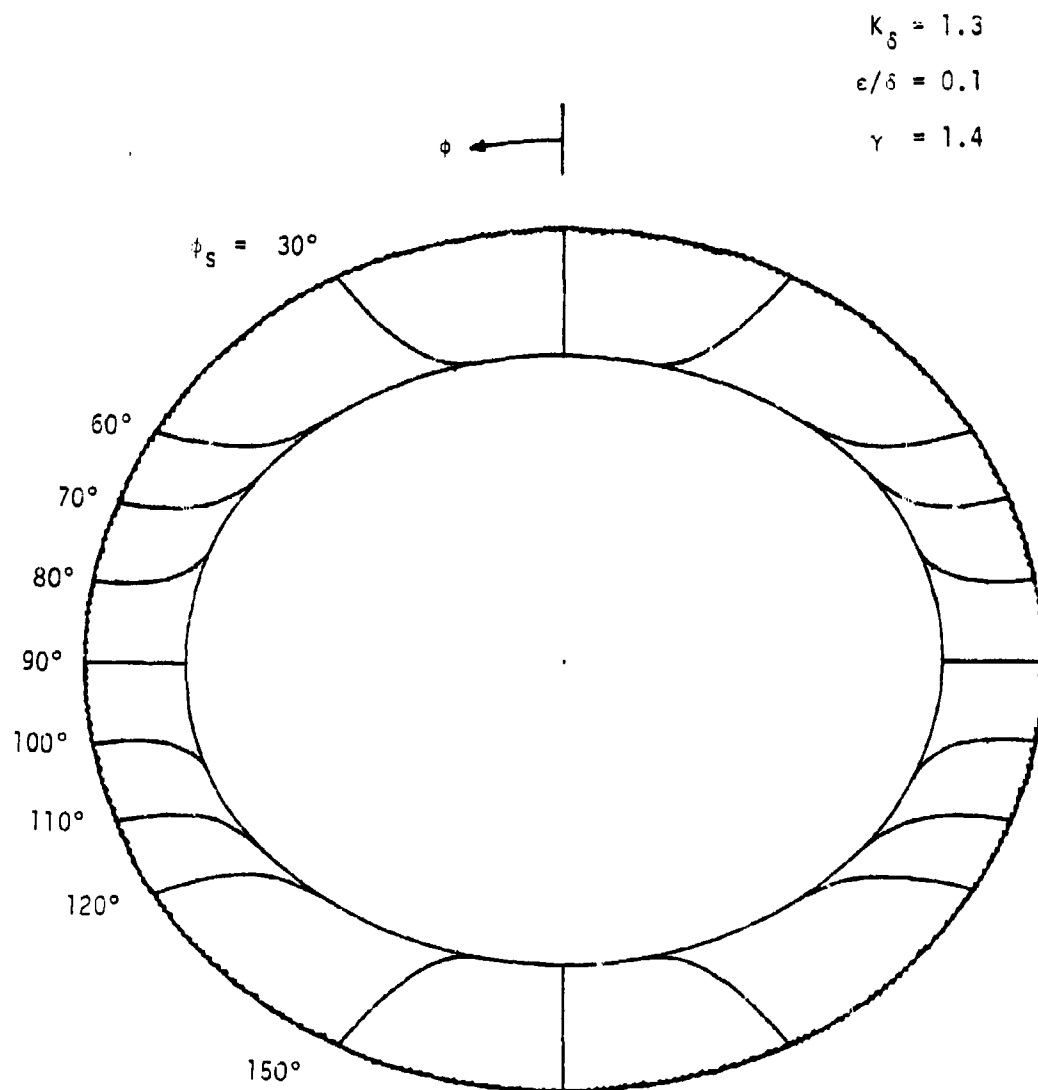


Figure 5.1 Stream Surfaces for Elliptic Cone

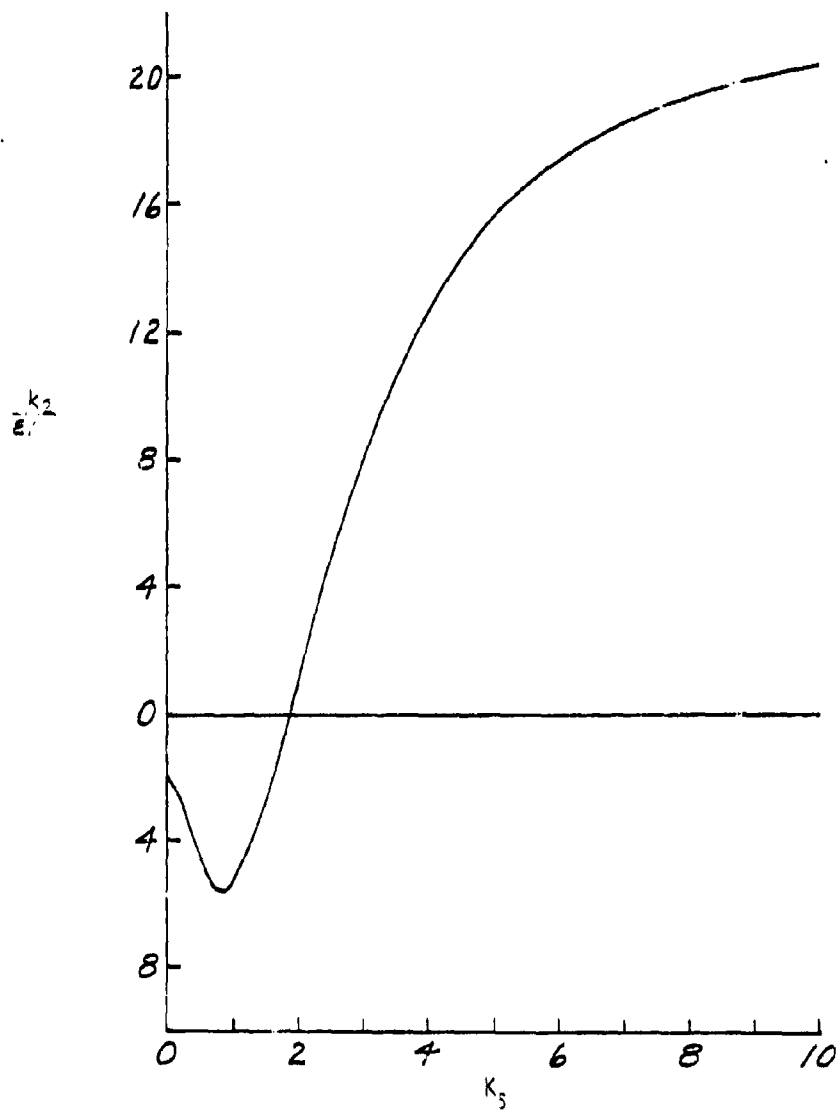


Figure 5.2 Elliptic-Cone Stream-Surface Function

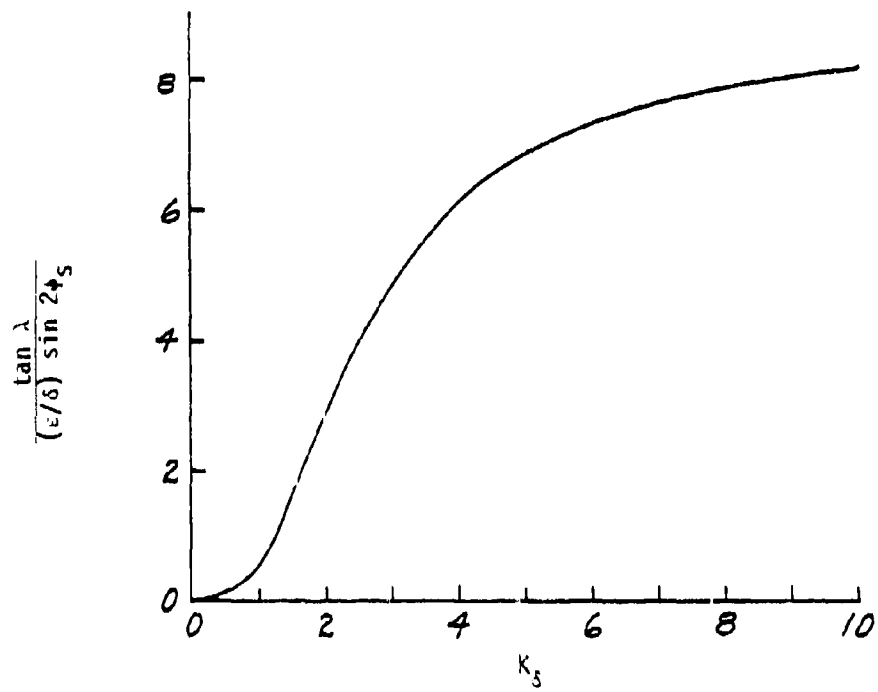
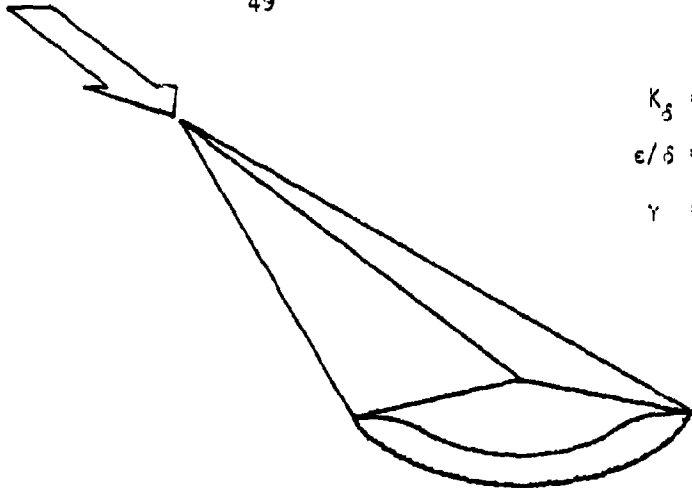


Figure 5.3 Elliptic-Cone Lip Angle

$$K_s = 1.3$$
$$\epsilon/\delta = 0.1$$
$$\gamma = 1.4$$


$$\phi_s = 100^\circ$$
$$\lambda = 2.2^\circ$$

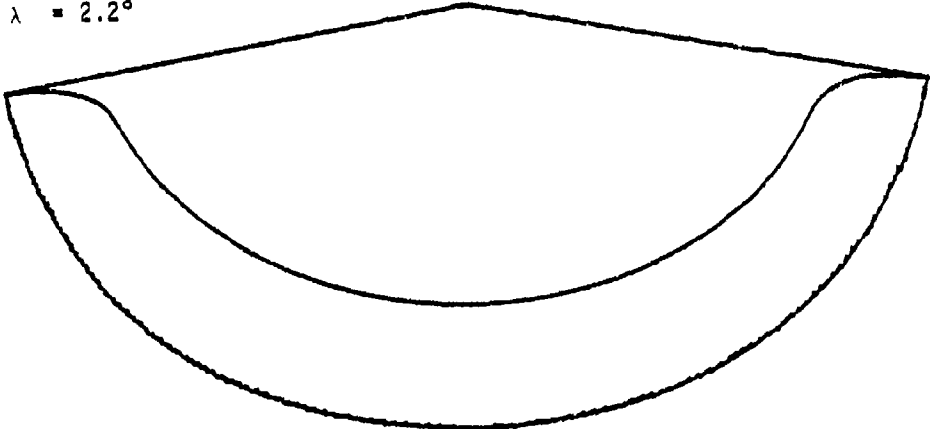

$$\phi_s = 110^\circ$$
$$\lambda = 4.0^\circ$$

Figure 5.4 Elliptic Cone Waveriders With Freestream Upper Surfaces

6. Waveriders Derived From Inclined Elliptic Cones

6.1 Stream Surfaces

The general stream-surface structure for flow past an inclined elliptic cone can be studied by rewriting Eq. (3.9) in the form

$$\frac{(\alpha\tilde{w}_1 + 2\varepsilon w_1)}{V_\infty(\theta^2 - \theta_c^2)} d\theta = \frac{d\mu}{(1 - \mu^2)(k_3 + k_4\mu)} \quad (6.1)$$

where $\mu \equiv \cos \phi$ (6.2a)

$$k_3 \equiv \frac{\alpha\tilde{w}_1(\theta)}{\alpha\tilde{w}_1(\theta) + 2\varepsilon w_1(\theta)} \quad (6.2b)$$

$$k_4 \equiv \frac{2\varepsilon w_1(\theta)}{\alpha\tilde{w}_1(\theta) + 2\varepsilon w_1(\theta)} \quad (6.2c)$$

The difficulty with the integration of Eq. (6.1) comes from the combination

$$w^*(\theta, \mu) \equiv k_3 + k_4\mu \quad (6.3)$$

which may vanish in the shock layer. The azimuthal velocity vanishes between the shock and the body when $w^* = 0$. The azimuthal location ϕ_0 where w^* vanishes is determined by

$$\cos \phi_0 = - \frac{\alpha}{2\varepsilon} \frac{\tilde{w}_1(\theta)}{w_1(\theta)} \quad (6.4)$$

The surface for $w^* = 0$ (dashed curve) is shown in Fig. 6.1 for $K_3 = 1.3$, $\gamma = 1.4$, $\alpha/\delta = 0.2$, and $\varepsilon/\delta = 0.1$. The position where this surface intersects the body surface is denoted by $\phi_0 = \phi_{0c}$ and is determined by

$$\begin{aligned} \cos \phi_{0c} &= - \frac{\alpha}{2\varepsilon} \frac{\tilde{w}_1(\theta_c)}{w_1(\theta_c)} \\ &\approx - \frac{\alpha}{2\varepsilon} \frac{\tilde{w}_1(\delta)}{w_1(\delta)} \end{aligned} \quad (6.5)$$

For the conditions in Fig. 6.1 we have $\phi_{0c} = 127^\circ$. The surface for $w^* = 0$ lies on the windward side of the body. Between the body and the surface $w^* = 0$ the azimuthal velocity is positive, and it is negative between the $w^* = 0$ surface

and the shock. For other conditions, $\cos \phi_{oc}$ can be calculated with the use of Fig. 6.2, which shows the ratio $w_1(\delta)/\bar{w}_1(\delta)$ as a function of K_δ for $\gamma = 1.4$. Also shown is the ratio at the shock, $w_1(\beta)/\bar{w}_1(\beta)$. For a given value of K_δ , the ratio $w_1(\theta)/\bar{w}_1(\theta)$ increases from the shock value to the surface value.

We can obtain a straightforward approximate integration of Eq. (6.1) by treating k_3 and k_4 as constants. Experience shows that the best values to use for these constants are the values at the body. For this choice, the body surface conditions are correctly given, which is especially important for the position of the intersection of the windward-leeward dividing stream surface with the body, denoted by ϕ_{oc} .

With the left side of Eq. (6.1) evaluated as for the previous cases, we obtain the approximate integral of Eq. (6.1) to be

$$\left[\frac{\theta - \theta_c}{\theta_s^* - \theta_c} \cdot \frac{\theta_s^*}{\theta} \right]^{\bar{k}_1 + k_1} \left[\frac{\theta + \theta_c}{\theta_s^* + \theta_c} \cdot \frac{\theta_s^*}{\theta} \right]^{\bar{k}_2 + k_2} = \left[\frac{\tan \frac{\phi}{2}}{\tan \frac{\phi_s}{2}} \right]^{k_5} \left[\frac{\bar{k}_1 \csc \phi + k_1 \cot \phi}{\bar{k}_1 \csc \phi_s + k_1 \cot \phi_s} \right]^{k_6} \quad (6.6)$$

$$\text{where } k_5 \equiv \bar{k}_1 / (\bar{k}_1 - k_1) \quad (6.7a)$$

$$k_6 \equiv k_1 / (\bar{k}_1 - k_1) \quad (6.7b)$$

$$\theta_c \equiv \delta - \epsilon \cos 2\phi \quad (6.7c)$$

$$\theta_s^* \equiv \beta + \alpha \bar{g} \cos \phi_s - \epsilon g \cos 2\phi_s \quad (6.7d)$$

Equation (6.6) reduces to Eq. (4.6) or (5.7) in the separate limits $\epsilon \rightarrow 0$ and $\alpha \rightarrow 0$. If the conditions are such that $\bar{k}_1 = k_1$, then the appropriate limit must be taken on the right-hand side of Eq. (6.6), which corresponds

to setting $k_3 = k_4$ in the original differential equation (6.1).

Figure 6.1 shows stream surfaces generated by Eq. (6.6) for the conditions $K_\delta = 1.3$, $\gamma = 1.4$, $\alpha/\delta = 0.2$, and $\epsilon/\delta = 0.1$. The dividing stream surface which separates the flow that proceeds toward the leeward ray from the flow that proceeds toward the windward ray occurs at $\phi_s = 127^\circ$. This dividing surface is a plane surface in this approximation. The actual stream surfaces should appear slightly different near the dividing stream surface and toward the windward ray. In this region the actual stream surfaces have a negative value of azimuthal velocity at the shock and hence should slope towards the leeward direction before curving into the radial direction at the surface $w^* = 0$ and then curving further towards the windward ray as shown. The slope $(\partial\phi/\partial\theta)_{\phi_s}$ should actually be positive in the windward region whereas the approximation (6.6) yields a slightly negative slope. Because the details of the azimuthal velocity field have not been taken into account, the dividing stream surface and its intersection with the body surface are not precisely described by the plane surface shown, even though the location of the body intersection is correct. Both the actual slopes and the approximation slopes at the shock are small in the windward region, and hence the description shown in Fig. 6.1 is qualitatively valid except for the aforementioned discrepancies.

6.2 Maximum-Entropy Surface

Outside the vortical and viscous boundary layers, the entropy has the expansion

$$s(\theta, \phi) = s_0(\theta) + \alpha \tilde{s}_1 \cos \phi + \epsilon s_1 \cos 2\phi, \quad (6.8)$$

where \tilde{s}_1 and s_1 are constants associated with the angle-of-attack and eccentricity perturbations. Let

$$s_1^* = \alpha \tilde{s}_1 \cos \phi_s + \epsilon s_1 \cos 2\phi_s \quad (6.9)$$

denote the entropy perturbation at the shock. It can be shown [11,13] that

$$\frac{s_1^*}{c_V} = -\gamma(\gamma-1) \beta (1-\xi_0)^2 \frac{V_\infty^2}{a_0^2(\beta)} [\alpha(1-\bar{g}) \cos \phi_s + \epsilon g \cos 2\phi_s] \quad (6.10)$$

where $\xi_0 = \rho_\infty/\rho_0(\beta)$ and $a_0^2(\beta) = \gamma P_0(\beta)/\rho_0(\beta)$. The maximum entropy perturbation at the shock occurs where the derivative with respect to ϕ_s of Eq. (6.10) vanishes. This occurs where

$$\cos \phi_{sm} = -\frac{\alpha(1-\bar{g})}{4 \epsilon g} \quad (6.11)$$

If the value of the right side is less than or equal to minus unity, the maximum occurs at the windward ray, $\phi_s = 180^\circ$. For the conditions of Fig. 6.1 ($K_s = 1.3$, $\gamma = 1.4$, $\alpha/\delta = 0.2$, $\epsilon/\delta = 0.1$), the maximum-entropy stream surface originates at the shock at $\phi_s = 133^\circ$. This is on the windward side of the dividing stream surface which is located in Fig. 6.1 at $\phi_s = 127^\circ$. Thus the maximum-entropy stream surface does not wet the body surface but lies in the windward part of the shock layer. That the body surface and maximum-entropy surface are not necessarily identical is also true for hypersonic blunt-body flows (see Hayes and Probstein [18], page 399). Melnik [10], on the other hand, in his analysis of conical flows assumed that the body was a maximum entropy surface. The conical result holds for all values of K_s . The ratio of $\cos \phi_{sm}$ and $\cos \phi_{oc}$, given by Eq. (6.5) is

$$\frac{\cos \phi_{sm}}{\cos \phi_{oc}} = \frac{1 - \bar{g}}{2g} \frac{w_1(\beta)}{\bar{w}_1(\delta)} \quad (6.12)$$

For $\gamma = 1.4$ this ratio is greater than unity for $K_s > 0$, and hence we conclude that $\phi_{sm} > \phi_{oc}$ for $K_s > 0$.

6.3 Lip Angle

Corresponding to Eqs. (4.12) and (5.10), we determine the lip angle, λ^* , for the shock-stream surface intersection for an inclined elliptic cone

to be given by

$$\begin{aligned}\tan \lambda^* &= \tan \bar{\lambda} + \tan \lambda \\ &= \frac{\alpha}{\delta} \frac{\sigma^2 - \bar{g}}{\sigma(\sigma^2 - 1)} \sin \phi_s + \frac{\epsilon}{\delta} \frac{2g}{\sigma(\sigma^2 - 1)} \sin 2\phi_s\end{aligned}\quad (6.13)$$

When the angles are small, the lip angle for an inclined elliptic-cone stream surface is equal to the sum of the lip angles for the corresponding inclined circular-cone stream surface and the aligned elliptic-cone stream surface.

6.4 Waveriders With Freestream Upper Surfaces

As before, waverider configurations can be formed by utilizing freestream plane surfaces that pass through the vertex along an axis inclined at an angle α with the cone axis, and intersect the shock at the lips of an underneath conical stream surface. As an example we choose the conditions shown in Fig. 6.1 with the lip located at $\phi_s = 90^\circ$. The waverider so formed is shown in Fig. 6.3. The freestream surface intersecting the shock at ϕ_s has a unit normal vector given by

$$\hat{n}_\infty = \frac{[\sigma - (\frac{\alpha}{\delta})(1-\bar{g}) \cos \phi_s - (\frac{\epsilon}{\delta}) g \cos 2\phi_s] \hat{e}_\phi - \frac{\alpha}{\delta} \sin \phi_s \hat{e}_\theta}{\sqrt{[\sigma - (\frac{\alpha}{\delta})(1-\bar{g}) \cos \phi_s - (\frac{\epsilon}{\delta}) g \cos 2\phi_s]^2 + (\frac{\alpha}{\delta})^2 \sin^2 \phi_s}}\quad (6.14)$$

The waverider lip angle, λ_w , is determined by the condition $\cos \lambda_w = \hat{n}_\infty \cdot \hat{n}$, where \hat{n} is given by Eq. (4.9). For small α/δ , we obtain

$$\tan \lambda_w = \tan \lambda^* + \frac{\frac{\alpha}{\delta} \sin \phi_s}{\sigma - (\frac{\alpha}{\delta})(1-\bar{g}) \cos \phi_s - (\frac{\epsilon}{\delta}) g \cos 2\phi_s}\quad (6.15)$$

The waverider lip angle in Fig. 6.3 is found to be $\lambda_w = 8.9^\circ$. This waverider has a positive dihedral and is analogous to the circular cone waverider shown in Fig. 4.4. The elliptic-cone waverider in Fig. 6.3 is more shallow

and flatter on the bottom than its circular-cone counterpart in Fig. 4.4. It also has a slightly greater span since the attached shock is broader for the ellipse. The pressure on the windward ray of the elliptic-cone waverider is less than that of its circular-cone counterpart, but the pressure at the lips is greater owing to the greater inclination of the shock. There are also elliptic cone waveriders with zero and negative dihedral, corresponding to the circular-cone waveriders shown in Figs. 4.5 and 4.6, but these will not be discussed here.

6.5 Further Remarks

Elliptic waveriders with wedge-shock upper surfaces can also be constructed, such as was done for the circular cone configuration shown in Fig. 4.7. Because there is an additional parameter, ϵ/δ , involved in fitting the wedge-shock to the waverider, the analysis is very involved and will not be considered here.

Other characteristics of interest for the families of waveriders presented here are lift, drag, and stability. The pressure coefficient on the conical stream surface can be obtained from the equation

$$\frac{C_p}{\delta^2}(\theta, \delta) = \frac{C_{p_0}(\theta)}{\delta^2} + \left(\frac{\alpha}{\delta}\right) \frac{\tilde{C}_{p_1}(\theta)}{\delta} \cos \phi + \left(\frac{\epsilon}{\delta}\right) \frac{C_{p_1}(\theta)}{\delta} \cos 2\phi, \quad (6.16)$$

which is in hypersonic similarity form and can be regarded as known [13,14]. The lift and drag characteristics can thus be determined without great difficulty. The pitching moment can also be determined, but general stability characteristics require a knowledge of off-design flow conditions. These considerations are fruitful subjects for further research.

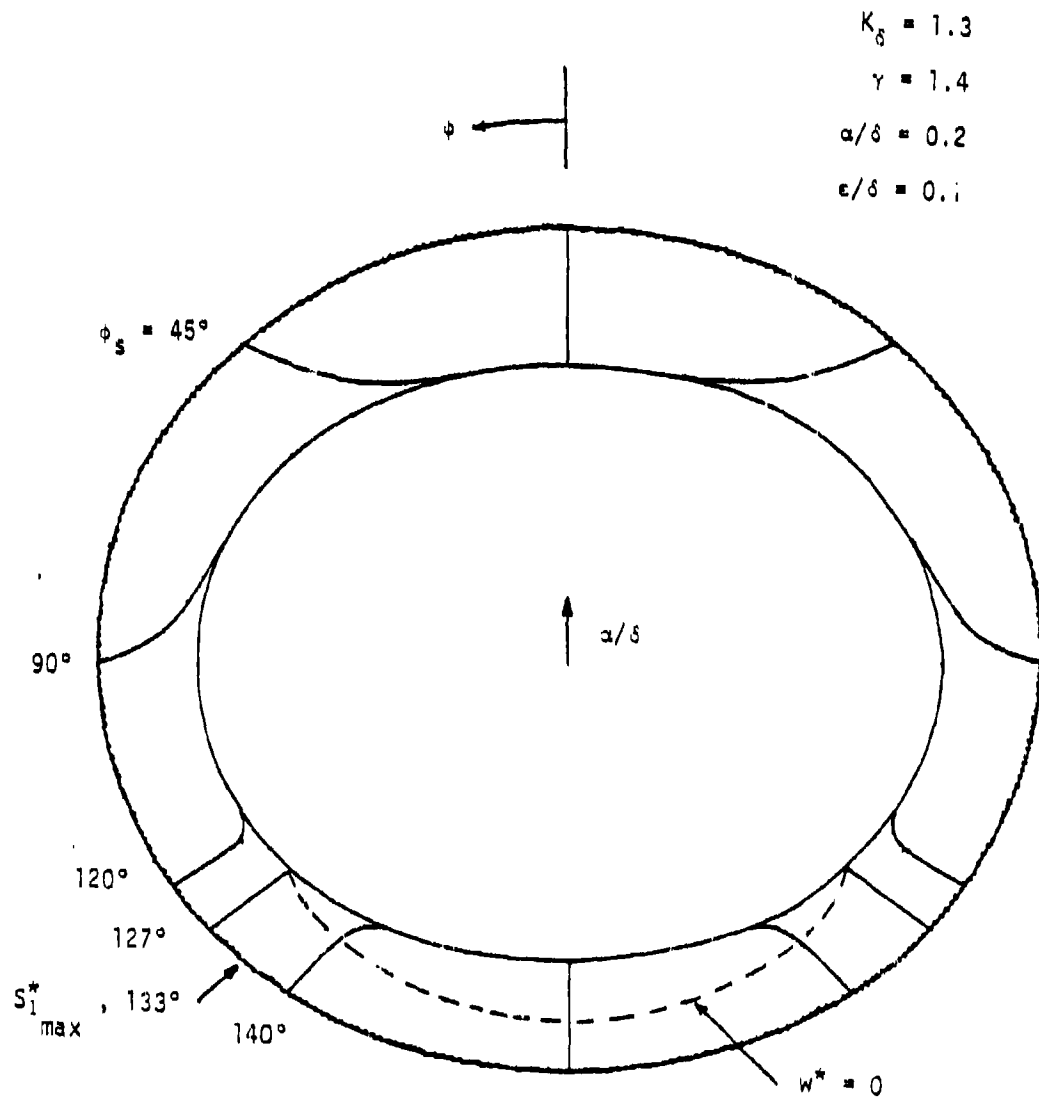


Figure 6.1 Stream Surfaces for Inclined Elliptic Cone

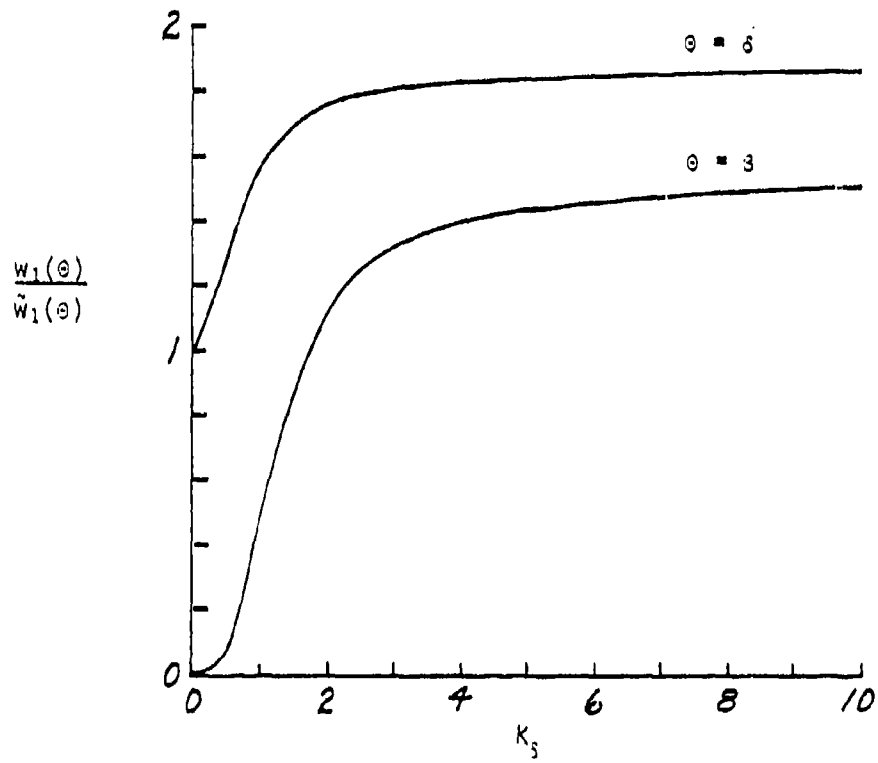


Figure 6.2 Azimuthal Velocity Ratios at Shock and Body

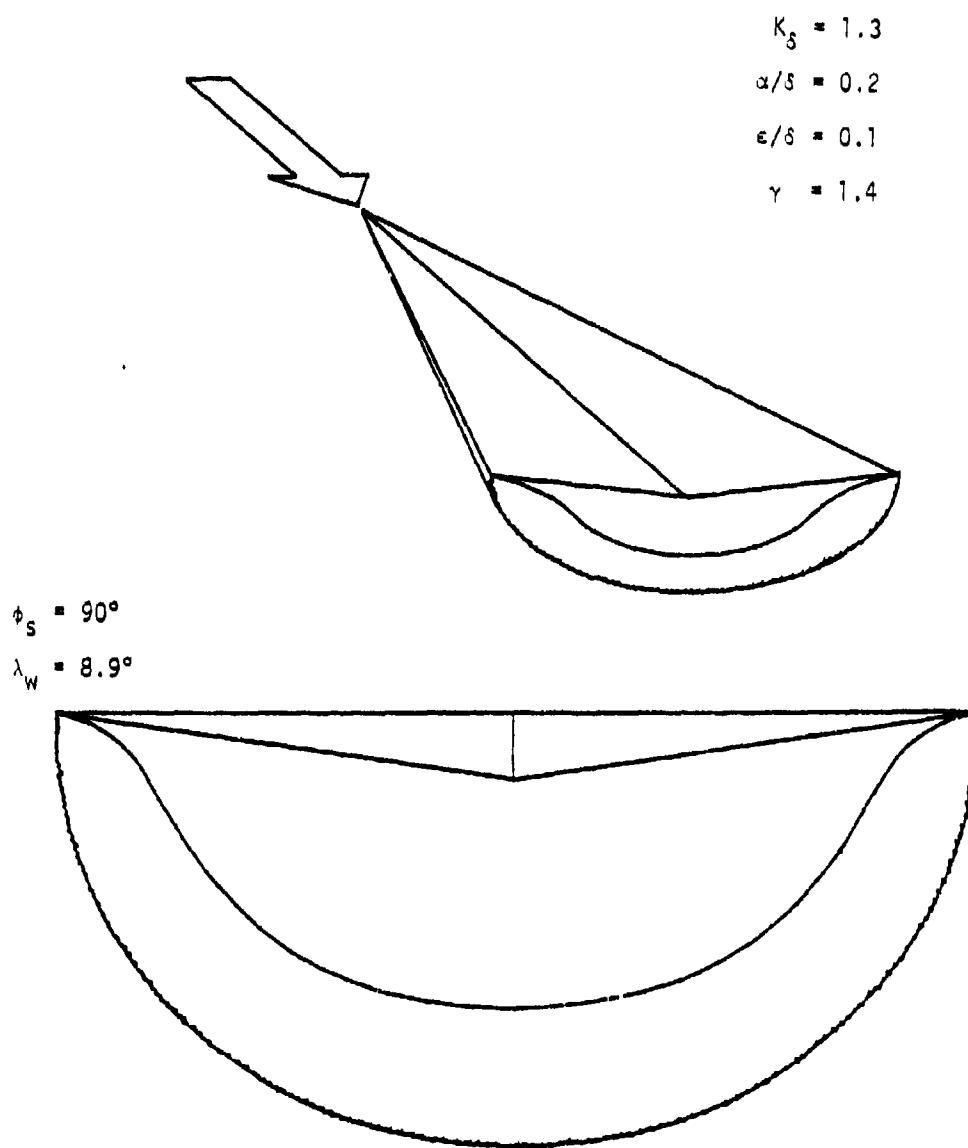


Figure 6.3 Inclined Elliptic-Cone Waverider With Freestream
Upper Surface: Positive Dihedral

7. Some Considerations Regarding Control Surfaces

7.1 Control Flaps

For controlled flight, control surfaces are necessary for changing and maintaining pitching, yawing, and rolling motions as well as aerodynamic trim. The waverider configurations that have been derived so far generally have horizontal or nearly horizontal surfaces where flaps can be placed to produce nearly vertical forces by their deflections. If enough dihedral is present, it may be possible that the flaps could produce the behavior of a vee tail and thus obviate the need of a vertical fin. In general, however, the design of controlled flight necessitates the consideration of vertical control surfaces. In this section we shall formulate the analysis of vertical fins that are themselves waverider configurations.

7.2 Vertical-Fin Control Surfaces

We consider a wedge-shock caret waverider, such as shown in Figs. 2a and 2b, but that is nonsymmetric, that is, the polar angles describing the free-stream surfaces are unequal. A typical configuration that shall be utilized as a vertical fin is shown in Fig. 7.1. Let one freestream surface be denoted by $\tan \theta_{s_{\infty}} = \theta_{s_{\infty}}$ (for small angles) to represent the angle between a freestream cone axis and the corresponding cone shock. The other freestream surface which shall represent the left half of a vertical fin is denoted by the conical angle θ_f . The flow deflection angle is denoted by Δ and the shock angle is denoted by β_w . All these polar angles are regarded as small and are shown as projections on a fixed Z plane. The dihedral angle between the two freestream surfaces is denoted by ψ_{∞} .

From geometrical considerations, the law of cosines yields

$$\Theta_{S_\infty}^2 - 2\Theta_{S_\infty}\Theta_f \cos \psi_\infty + \Theta_f^2 = [(\Theta_{S_\infty}^2 - \beta_W^2)^{1/2} + (\Theta_f^2 - \beta_W^2)^{1/2}]^2. \quad (7.1)$$

Expanding this equation and solving for Θ_f yields

$$\frac{\Theta_{S_\infty}}{\Theta_f} = \cos \psi_\infty \pm \sin \psi_\infty \left[\left(\frac{\Theta_{S_\infty}}{\beta_W} \right)^2 - 1 \right]^{1/2}. \quad (7.2)$$

Since $\Theta_{S_\infty}/\Theta_f$ is always positive the plus sign must be chosen when $\psi_\infty > 90^\circ$ since $\cos \psi_\infty$ is then negative. For a continuous variation, a change in sign occurs when the radical vanishes. This does not occur since $\Theta_{S_\infty}/\beta_W > 1$. Hence the plus sign is to be selected in Eq. (7.2).

Equation (7.2) follows from the geometry of the configuration. The shock conditions of gas dynamics, however, require that β_W is determined by the flow deflection Δ and the freestream Mach number as given by Eq. (2.1). We can thus rewrite Eq. (7.2) as

$$\frac{\Theta_{S_\infty}}{\Theta_f} = \cos \psi_\infty + \sin \psi_\infty \left[\left(\frac{\Theta_{S_\infty}}{\delta} \right)^2 \left(\frac{\delta}{\beta_W} \right)^2 - 1 \right]^{1/2}, \quad (7.3)$$

and determine δ/β_W from

$$\frac{\delta}{\beta_W} = K_\delta \left[-\frac{\gamma+1}{4} K_\delta \left(\frac{\Delta}{\delta} \right) + \sqrt{\left(\frac{\gamma+1}{4} \right)^2 K_\delta^2 \left(\frac{\Delta}{\delta} \right)^2 + 1} \right]. \quad (7.4)$$

Thus (Θ_f/δ) is a function of Θ_{S_∞}/δ , K_δ , γ , $\cos \psi$, and Δ/δ , where δ is taken as the characteristic angle of the cone flow. When $\Delta = 0$, β_W takes the Mach angle as its minimum value, and Θ_f takes a minimum value given by

$$\frac{\Theta_{S_\infty}}{\Theta_{f \min}} = \cos \psi_\infty + \sin \psi_\infty \left[\left(\frac{\Theta_{S_\infty}}{\delta} \right)^2 K_\delta^2 - 1 \right]^{1/2}. \quad (7.5)$$

7.3 Vertical Fin for the Elliptic-Cone Waverider

We consider the elliptic-cone waveriders shown in Fig. 5.4 with the conditions $K_\delta = 1.3$, $\gamma = 1.4$, and $\epsilon/\delta = 0.1$. In this case we match the freestream upper surfaces of the cone waverider with the freestream surface of the half-fin analyzed in Section 7.2. We thus set $\psi_\infty = \phi_S$ and

$$\theta_{S_\infty} = \theta_S^* \equiv \beta - \epsilon \gamma \cos 2\phi_S \quad (7.6)$$

For the lip at $\phi_S = 100^\circ$, we get for various values of Δ/δ

Δ/δ	θ_{S_∞}/δ
0	1.06
0.1	1.21
0.2	1.40

Since the freestream surfaces are matched, the vertical fin can start at the cone vertex, or at some other position. The configuration for which the fin starts at the vertex is shown in Fig. 7.2 for $\Delta/\delta = 0.2$. In this case the fin shock is attached to the conical lip. The case where the fin begins half-way back on the elliptic-cone undersurface is shown in Fig. 7.3 for $\Delta/\delta = 0.2$. In a real flow, owing to viscous boundary-layer shock interaction, the flow would not be as well-behaved as illustrated here.

7.4 Vertical Fin for Inclined-Cone Waveriders

When the basic conical waverider surfaces are derived from cones at angle-of-attack, the freestream surfaces are inclined at an angle α with the geometric cone axis. The formulas in Section 7.2 must be adapted to these situations by the appropriate evaluation of ψ_∞ and θ_{S_∞} . The unit normal vector to the freestream surface passing through lip shock and the freestream cone axis is given by \hat{n}_∞ , defined by Eq. (6.14). If \hat{e}_y denotes the unit normal vector to the

vertical plane, then we obtain ψ_∞ from the condition $\cos \psi_\infty = -\hat{n}_\infty \cdot \hat{e}_y$

$$\cos \psi_\infty = \frac{[\sigma - (\frac{\alpha}{\delta})(1-\bar{g}) \cos \phi_s - (\frac{\epsilon}{\delta}) \bar{g} \cos 2\phi_s] \cos \phi_s + \frac{\alpha}{\delta} \sin^2 \phi_s}{\sqrt{[\sigma - (\frac{\alpha}{\delta})(1-\bar{g}) \cos \phi_s - (\frac{\epsilon}{\delta}) \bar{g} \cos 2\phi_s]^2 + (\frac{\alpha}{\delta})^2 \sin^2 \phi_s}} \quad (7.7)$$

When $\alpha = 0$, this reduces to the result $\psi_\infty = \pi - \phi_s$. There is no discrepancy in this result compared to Section 7.3 if it is realized that the windward ray was taken as $\phi = 0$ for the inclined-cone waveriders, whereas the non-inclined elliptic-cone waverider utilized $\phi_s > \pi/2$ for the conical surface.

From geometrical considerations, we also obtain

$$\theta_{s_\infty} = [\theta_s^*{}^2 + \alpha^2 - 2\theta_s^* \alpha \cos \phi_s]^{1/2}, \quad (7.8)$$

where

$$\theta_s^* = \beta + \alpha \bar{g} \cos \phi_s - 2\epsilon \bar{g} \cos 2\phi_s. \quad (7.9)$$

We shall not consider further calculations here.

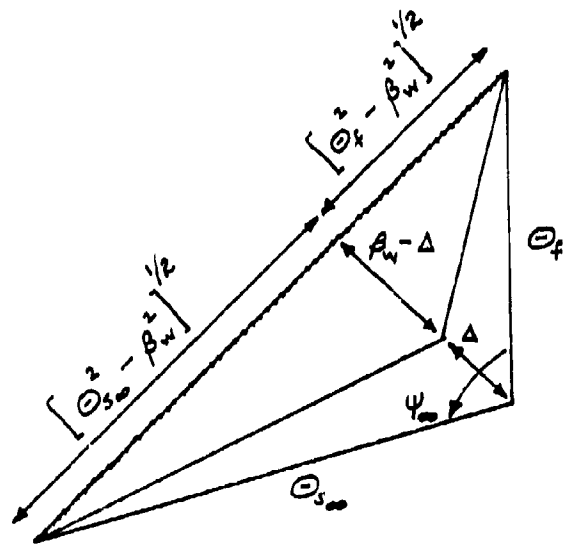


Figure 7.1 Geometry for the Vertical Fin

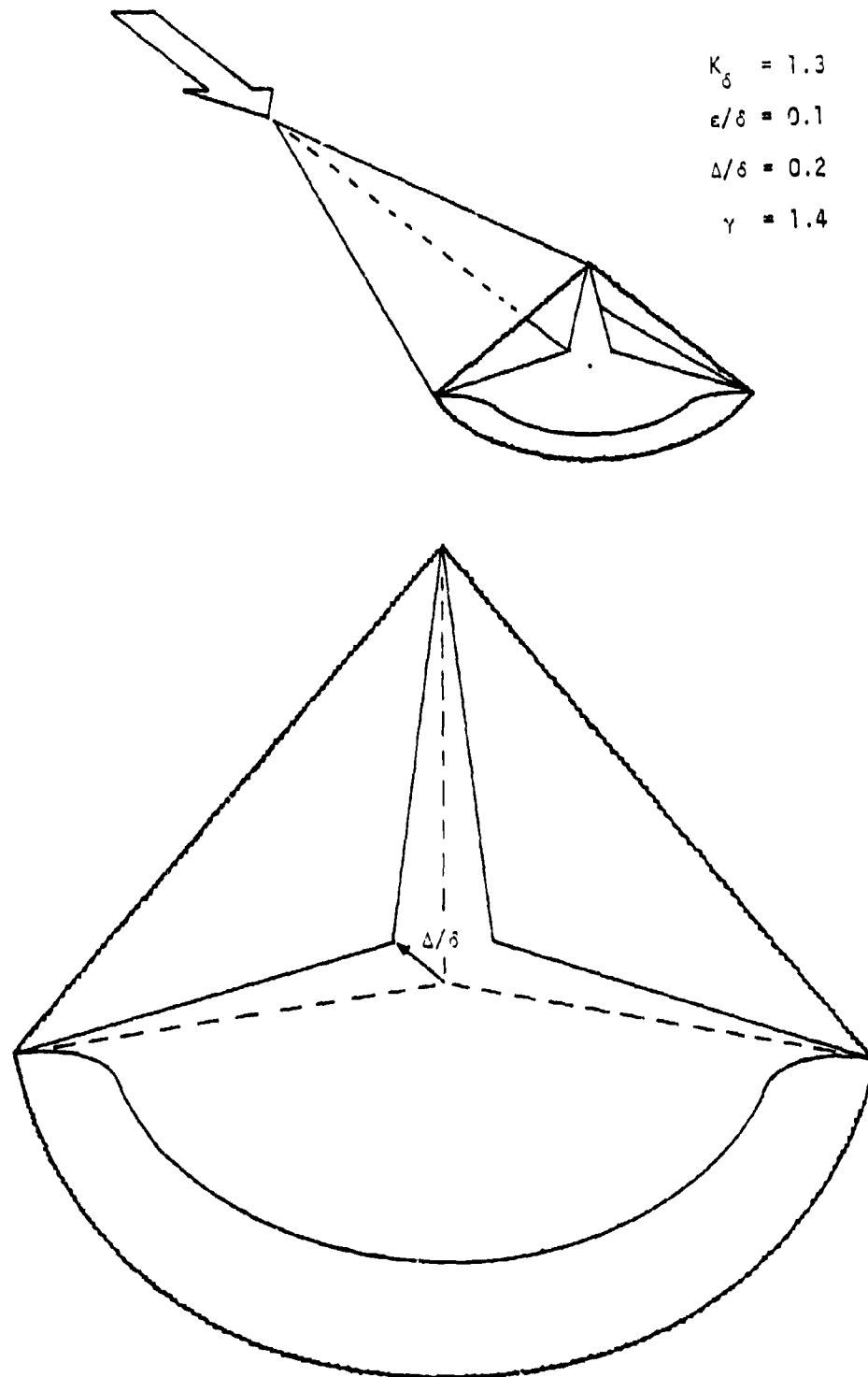


Figure 7.2 Elliptic-Cone Waverider with Fin Starting at Vertex

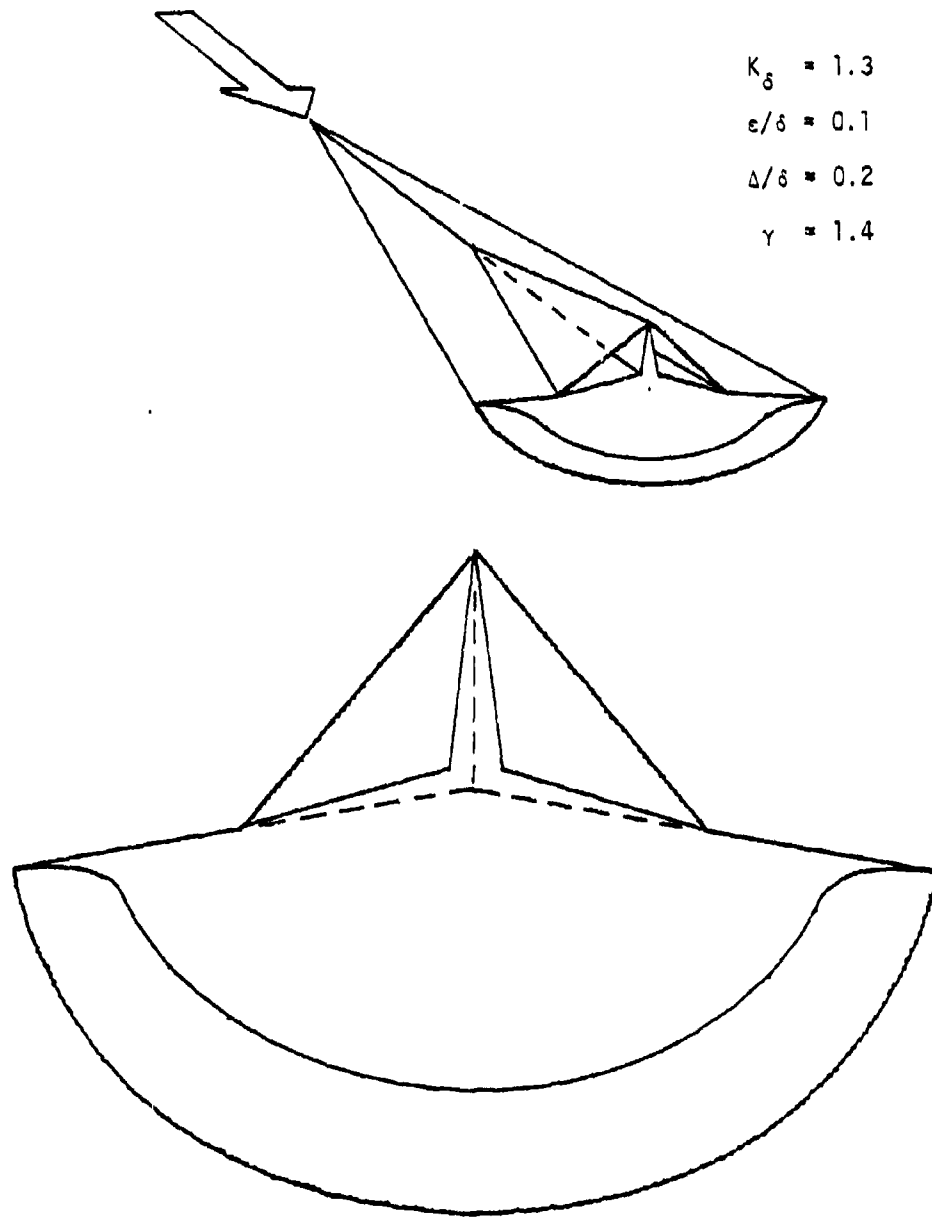


Figure 7.3 Elliptic-Cone Waverider with Fin Starting at Half Length

8. Concluding Remarks

By means of stream surfaces obtained from angle-of-attack and cross-section eccentricity perturbations of the basic supersonic axisymmetric flow past a circular cone, aerodynamic lifting-body configurations have been derived. The emphasis has been on a systematic parametric study on the various configurations that can be obtained. The configurations have attached shocks on sharp leading edges and thus can be described as conical waveriders. Utilization of wedge-shock caret-waverider results leads to a combination of configurations and to vertical-fin control surfaces. Generalization of the perturbed flow past a circular cone to allow for generalized non-circular cross sections [19] can lead to further aerodynamic combinations.

The analysis has proceeded within the framework of hypersonic small-disturbance theory, and approximate analytic formulas have been derived that apply over a wide range of conditions. Although pressure distributions have not been calculated, the pertinent formulas have been presented. Further calculations by interested investigators can be performed readily.

The lifting-body configurations that have been presented appear attractive in terms of high lift-drag ratio requirements. Further work is required to account for other aerodynamic factors. Some of these are

- 1) lift, drag, and moment characteristics,
- 2) boundary-layer growth and related viscous effects,
- 3) off-design effects,
- 4) details of flaps and other control surfaces,
- 5) unsteady flow and dynamic forces and moments,
- 6) blunted edges and noses,
- 7) experimental results.

These subjects are part of a continuing program of research at the University of Oklahoma, sponsored by the United States Air Force.

References

1. Küchemann, D. "Hypersonic Aircraft and Their Aerodynamic Problems." Progress in Aeronautical Sciences, Vol. 6, Edited by D. Küchemann and L. H. G. Stern. Pergamon Press, London, 1965, pg. 271.
2. Küchemann, D. and Weber, J. "An Analysis of Some Performance Aspects of Various Types of Aircraft Designed to Fly Over Different Ranges at Different Speeds." Progress in Aeronautical Sciences, Vol. 9, Edited by D. Küchemann et al. Pergamon Press, London, 1968, pg. 329.
3. Nonweiler, T. R. F. "Delta Wings of Shape Amenable to Exact Shock-Wave Theory." J. Roy. Aero. Soc. 67, 1963, pg. 39.
4. Venn, J. and Flower, J. W. "Shock Patterns for Simple Caret Wings." J. Roy. Aero. Soc. 74, 1970, pp. 339-348.
5. Nardo, C. T. "Aerodynamic Characteristics of Two-Dimensional Waverider Configurations." AIAA Journal, Vol. 10, No. 9, 1972, pg. 1258.
6. Jones, J. G. "A Method for Designing Lifting Configurations for High Supersonic Speeds Using the Flow Fields of Non-Lifting Cones." R.A.E. Report No. Aero 2674, A.R.C. 24846, 1963.
7. Woods, B. A. "The Construction of a Compression Surface Based on an Axisymmetrical Conical Flow Field." R.A.E. Tech. Note No. Aero 2900, A.R.C. 25087, 1963.
8. Cheng, H. K. "Hypersonic Flows Past a Yawed Circular Cone and Other Pointed Bodies." Journal of Fluid Mechanics, Vol. 12, 1962, pp. 169-191.
9. Munson, A. G. "The Vortical Layer on an Inclined Cone." Journal of Fluid Mechanics, Vol. 20, 1964, pp. 625-643.
10. Melnik, R. E. "Vortical Singularities in Conical Flow." AIAA Journal, Vol. 5, No. 4, 1967, pp. 631-637.
11. Doty, R. T. "Hypersonic Flow Past an Inclined Cone." M.S. Thesis, Aerospace, Mechanical and Nuclear Engineering, University of Oklahoma, 1972.
12. Doty, R. T. and Rasmussen, M. L. "Approximation for Hypersonic Flow Past an Inclined Cone." AIAA Journal, Vol. 11, No. 9, 1973, pp. 1310-1315.
13. Lee, H. M. and Rasmussen, M. L. "Hypersonic Flow Past a Slender Elliptic Cone." University of Oklahoma, School of Aerospace, Mechanical and Nuclear Engineering Research Report No. OU-AMNE-78-2, 1978.

14. Rasmussen, M. L. and Lee, H. M. "Approximation for Hypersonic Flow Past a Slender Elliptic Cone." AIAA Paper No. 79-0364, AIAA 17th Aerospace Sciences Meeting, New Orleans, January, 1979.
15. Squire, L. C. "The Aerodynamics of Lifting Bodies at High Supersonic Speeds." J. Roy. Aero. Soc. 75, 1971, pg. 18.
16. Linnell, R. D. "Two-Dimensional Airfoils in Hypersonic Flows." Journal of Aeronautical Sciences, Vol. 16, 1949, pp. 22-30.
17. Rasmussen, M. L. "On Hypersonic Flow Past an Unyawed Cone." AIAA Journal, Vol. 5, No. 8, 1967, pp. 1495-1497.
18. Hayes, W. D. and Probstein, R. F. Hypersonic Flow Theory, Vol. I, Inviscid Flows. Second Edition. Academic Press, New York, 1966.
19. Jischke, Martin C. "Supersonic Flow Past Conical Bodies with Nearly Circular Cross Sections." University of Oklahoma, School of Aerospace, Mechanical and Nuclear Engineering Research Report No. OU-AMNE-78-10, October, 1978.

APPENDIX A
FORMULAS FOR THE BASIC AXISYMMETRIC CONE FLOW

Formulas for the hypersonic flow field in the shock layer of an unyawed cone can be obtained from the analysis of Rasmussen [17]. They are also derived alternatively in the Appendix of reference [11]. For small angles within the framework of hypersonic small-disturbance theory, the radial and polar velocity components are given approximately by

$$\frac{u_0}{V_\infty} = 1 - \frac{\delta^2}{2} \left[\frac{\theta^2}{\delta^2} + \ln \frac{\beta^2}{\theta^2} \right] , \quad (\text{A.1})$$

$$\frac{v_0}{V_\infty} = -\theta \left[1 - \frac{\delta^2}{\theta^2} \right] , \quad (\text{A.2})$$

where

$$\frac{\beta}{\delta} = \left[\frac{\gamma+1}{2} + \frac{1}{K_\delta^2} \right]^{1/2} . \quad (\text{A.3})$$

and $K_\delta \equiv M_\infty \delta$ is the hypersonic small-disturbance parameter.

The temperature, speed of sound, and Mach number are given in terms of the velocity for homentropic and homenergetic flow. We obtain

$$\frac{T_0}{T_\infty} = \frac{a_0^2}{a_\infty^2} = \frac{(\gamma-1) M_\infty^2 + 2}{(\gamma-1) M_0^2 + 2} = 1 + \frac{\gamma-1}{2} K_\delta^2 \left[2 + \ln \frac{\beta^2}{\theta^2} - \frac{\delta^2}{\theta^2} \right] , \quad (\text{A.4})$$

where errors of order δ^2 have been ignored. Since the flow is homentropic, the pressure is determined by

$$\frac{p_0(\theta)}{p_0(\beta)} = \left[\frac{T_0(\theta)}{T_0(\beta)} \right]^{\frac{\gamma}{\gamma-1}} = \left[1 + \frac{T_0(\theta) - T_0(\beta)}{T_0(\beta)} \right]^{\frac{\gamma}{\gamma-1}} . \quad (\text{A.5})$$

The temperature change (and hence the pressure change) across the shock layer is small, and hence we can use the first term of a binomial expansion to write

$$\frac{p_0(\theta)}{p_0(\beta)} \approx 1 + \frac{\gamma}{\gamma-1} \frac{T_0(\theta) - T_0(\beta)}{T_0(\beta)} . \quad (\text{A.6})$$

When the pressure jump across the shock is taken into account,

$$\begin{aligned} \frac{p_0(\beta)}{p_\infty} &= 1 + \frac{2\gamma}{\gamma-1} (M_\infty^2 \sin^2 \beta - 1) , \\ &\approx 1 + \gamma K_\delta^2 , \end{aligned} \quad (A.7)$$

we can finally write the pressure distribution across the shock layer as

$$\frac{p_0(\theta)}{p_\infty} = 1 + \frac{\gamma K_\delta^2}{2} \left[1 + \frac{(\gamma+1) K_\delta^2 + 2}{(\gamma-1) K_\delta^2 + 2} \left\{ 1 - \frac{\delta^2}{\theta^2} + \ln \frac{\beta^2}{\theta^2} \right\} \right] . \quad (A.8)$$

APPENDIX B

FORMULAS FOR THE INCLINED ELLIPTIC CONE FLOW PERTURBATIONS

The flow perturbations outside the vortical layer are a linear combination of the angle-of-attack contribution and the cross-section eccentricity contribution, as given by Eqs. (3.6). At the shock, the angle-of-attack velocity perturbations are given by [11,12]

$$\frac{\tilde{u}_1(\beta)}{V_\infty} \cong [1 - \tilde{g}(1 - \xi_0)] \quad , \quad (\text{B.1})$$

$$\frac{\tilde{v}_1(\beta)}{V_\infty} \cong (1 - \tilde{g}) \left[2 \frac{(\gamma - 1)}{\gamma + 1} - \xi_0 \right] + \tilde{g}(2 - \xi_0) \quad , \quad (\text{B.2})$$

$$\frac{\tilde{w}_1(\beta)}{V_\infty} \cong - [1 - \tilde{g}(1 - \xi_0)] \quad , \quad (\text{B.3})$$

where

$$\xi_0 \equiv \frac{\rho_\infty}{\rho_0(\beta)} = 1 - \frac{\delta^2}{\beta^2} = \frac{\sigma^2 - 1}{\sigma^2} \quad (\text{B.4})$$

is the density ratio, and $\sigma \equiv \beta/\delta$. The shock eccentricity factor is given by

$$\tilde{g} = \frac{3 + 2\sigma^2 \left[3 - \frac{4(1 + \sigma^2)}{\gamma + 1} \right] - \frac{\ln[\sigma + \sqrt{\sigma^2 - 1}]}{\sigma \sqrt{\sigma^2 - 1}}}{5 - 2(1 + \sigma^2) \left[1 + \frac{4\sigma^2}{\gamma + 1} \right] - \frac{\ln[\sigma + \sqrt{\sigma^2 - 1}]}{\sigma \sqrt{\sigma^2 - 1}}} \quad (\text{B.5})$$

At the shock, the cross-section eccentricity velocity perturbations are given by [13,14]

$$\frac{u_1(\beta)}{V_\infty} = g \beta (1 - \xi_0) \quad , \quad (\text{B.6})$$

$$\frac{v_1(\beta)}{V_\infty} = g \left[\left\{ \frac{2(\gamma-1)}{\gamma+1} - \xi_0 \right\} - (2 - \xi_0) \right] \quad , \quad (\text{B.7})$$

$$\frac{w_1(\beta)}{V_\infty} = -2g (1 - \xi_0) \quad , \quad (\text{B.8})$$

and the shock eccentricity factor is given by

$$g = \frac{6\sigma^3}{\frac{3 \cos^{-1} \left(\frac{1}{\sigma} \right)}{\sqrt{\sigma^2-1}} + \frac{6}{\gamma+1} (\sigma^6 + \sigma^2) + 3\sigma^4 - \sigma^2 - 5} \quad . \quad (\text{B.9})$$

The pressure disturbance in the shock layer is given by [11,12,13,14]

$$\frac{\tilde{p}_1(\theta)}{p_0(\theta)} = -\gamma (u_0 \tilde{u}_1 + v_0 \tilde{v}_1) / a_0^2 + \tilde{F}_1 \quad , \quad (\text{B.10a})$$

$$\frac{p_1(\theta)}{p_0(\theta)} = -\gamma (u_0 u_1 + v_0 v_1) / a_0^2 + F_1 \quad , \quad (\text{B.10b})$$

where

$$\tilde{F}_1 = -\frac{\tilde{s}_1}{(\gamma-1)C_V} = \gamma V_\infty^2 \beta (1-\tilde{g})(1-\xi_0)^2 / a_0^2 (\beta) \quad , \quad (\text{B.11a})$$

$$F_1 = -\frac{s_1}{(\gamma-1)C_V} = \gamma V_\infty^2 \beta g(1-\xi_0)^2 / a_0^2 (\beta) \quad . \quad (\text{B.11b})$$

The azimuthal velocity perturbation $w_1(\theta)$ is related to the radial perturbation $u_1(\theta)$ by [13,14]

$$n u_1(\theta) + \theta w_1(\theta) = \frac{n F_1}{\gamma} H_0(\theta) \quad , \quad (\text{B.12})$$

where

$$H_0(\theta) = \frac{1}{I} \int_{\beta}^{\theta} \frac{a_0^2 I}{v_0} d\theta \quad , \quad (\text{B.13a})$$

$$I \equiv \exp \left[\int_{\beta}^{\theta} \frac{u_0}{v_0} d\theta \right] , \quad (\text{B.13b})$$

and where $n = 1$ for the angle-of-attack perturbation and $n = 2$ for the cross-section eccentricity perturbation. The pressure at the body surface $\theta = \delta + 0(\alpha, \epsilon)$ does not depend on v_1 since $v_0(\delta) = 0$. Thus, replacing $u_1(\delta)$ by $w_1(\delta)$ by means of Eq. (B.12) yields the body pressure perturbation as a function of the azimuthal velocity perturbation:

$$\frac{p_1(\delta)}{p_0(\delta)} = \frac{\gamma \delta u_0(\delta) w_1(\delta)}{n a_0^2(\delta)} + F_1 \left[1 - \frac{u_0(\delta) H_0(\delta)}{a_0^2(\delta)} \right] . \quad (\text{B.14})$$

When $H_0(\delta)$ is evaluated by means of Eqs. (A.1) and (A.2) and it is noted that $a_0^2(\theta)$ varies only a small amount across the shock layer, such that $a_0^2(\theta) = a_0^2(\beta)$, then $H_0(\delta)$ has approximately the value [13,14]

$$H_0(\delta) = a_0^2(\beta) / V_{\infty} . \quad (\text{B.15})$$

Thus, since $u_0(\delta) / V_{\infty} = 1 + O(\delta^2)$, we can approximate Eq. (B.14) by

$$\frac{p_1(\delta)}{p_0(\delta)} = \frac{\gamma \delta V_{\infty} w_1(\delta)}{n a_0^2(\delta)} + F_1 \left[1 - \frac{a_0^2(\beta)}{a_0^2(\delta)} \right] . \quad (\text{B.16})$$

The coefficient of F_1 is small enough to neglect, and we therefore obtain

$$\frac{p_1(\delta)}{p_0(\delta)} = \frac{\gamma \delta V_{\infty} w_1(\delta)}{n a_0^2(\delta)} . \quad (\text{B.17})$$

The pressure perturbation at the surface is thus very nearly proportional to the azimuthal velocity. This result is consistent with the fact that both the pressure and first-order azimuthal velocity are uniformly valid across the vortical layer.

The azimuthal velocity perturbations evaluated at the surface have the values [11,12,13,14]

$$\frac{\tilde{w}_1(\delta)}{V_\infty} = - \left[- (1+\tilde{g}) + \frac{1-\tilde{g}}{2\sigma^2} \left(\frac{8\sigma^4}{\gamma+1} - 1 - \frac{\ln [\sigma + \sqrt{\sigma^2-1}]}{\sigma \sqrt{\sigma^2-1}} \right) \right] , \quad (\text{B.18})$$

$$\frac{w_1(\delta)}{V_\infty} = - g \left[\sigma - \frac{1}{3\sigma} + \frac{1}{3\sigma^3} + \frac{2}{\gamma+1} \left(\sigma^3 - \frac{1}{\sigma} \right) - \frac{\cos^{-1}(\frac{1}{\sigma})}{\sigma \sqrt{\sigma^2-1}} \right] . \quad (\text{B.19})$$

The perturbation pressure variation across the shock layer can be obtained from Eqs. (B.10) when \tilde{u}_1 , u_1 , \tilde{v}_1 , and v_1 are evaluated by the formulas of references [11,12,13,14]. Since the values of the pressure at the shock and at the body are given here, a simple linear variation with θ across the shock layer is adequate for design calculations.

REPORT DOCUMENTATION PAGE		READ INSTRUCTIONS BEFORE COMPLETING FORM
1. REPORT NUMBER AFOSR/TR-79-0474	2. GOVT ACCESSION NO.	3. RECIPIENT'S CATALOG NUMBER
4. TITLE (and Subtitle) LIFTING BODIES DERIVED FROM SUPERSONIC FLOWS PAST INCLINED CIRCULAR AND ELLIPTIC CONES		5. TYPE OF REPORT & PERIOD COVERED Final Scientific PART II
7. AUTHOR(s) Maurice L/Rasmussen		6. CONTRACT OR GRANT NUMBER(s) AFOSR-77-3468
9. PERFORMING ORGANIZATION NAME AND ADDRESS Aerospace, Mechanical & Nuclear Engineering University of Oklahoma Norman, Oklahoma 73019		10. PROGRAM ELEMENT, PROJECT, TASK AREA & WORK UNIT NUMBERS 2301/A6/ 61102F
11. CONTROLLING OFFICE NAME AND ADDRESS AFOSR/NF Boiling AFB Wash DC 20332		12. REPORT DATE Dec 1978
14. MONITORING AGENCY NAME & ADDRESS (if different from Controlling Office)		13. NUMBER OF PAGES 82
16. DISTRIBUTION STATEMENT (of this Report) Approved for public release; distribution unlimited.		15. SECURITY CLASS. (of this report) unclassified
		15a. DECLASSIFICATION/DOWNGRADING SCHEDULE
17. DISTRIBUTION STATEMENT (of the abstract entered in Block 20, if different from Report) DISTRIBUTION STATEMENT A Approved for public release; Distribution Unlimited		
18. SUPPLEMENTARY NOTES		
19. KEY WORDS (Continue on reverse side if necessary and identify by block number)		
20. ABSTRACT (Continue on reverse side if necessary and identify by block number) Lifting-body configurations are constructed from stream surfaces generated by means of supersonic flows past inclined circular and elliptic cones. By such means waverider shapes are devised with curved surfaces and known pressure fields and shock-layer structures. The conical flow fields stem from perturbations of the basic axisymmetric cone flow arising from small angle of attack and small cross-section eccentricity. The approximate results are analytic and in the form of hypersonic small disturbance theory. Various possibilities for		

waverider shapes are discussed. Design formulas are presented that determine how the Mach number, angle of attack, cross-section eccentricity, and characteristic cone angle affect the waverider shape, pressure distribution, and shock-layer structure. N

UNCLASSIFIED